SUPPLEMENTARY MATERIALS

CHARACTERIZATION OF (1) – (3):

CRYSTALLOGRAPHY:

ELECTROCHEMISTRY

ELECTRONIC ABSORPTION SPECTRA AND DFT CALCULATION

PHOTOLUMINESCENCE PROPERTIES

BIOLOGICAL ACTIVITY

CHARACTERIZATION OF (1) – (3)

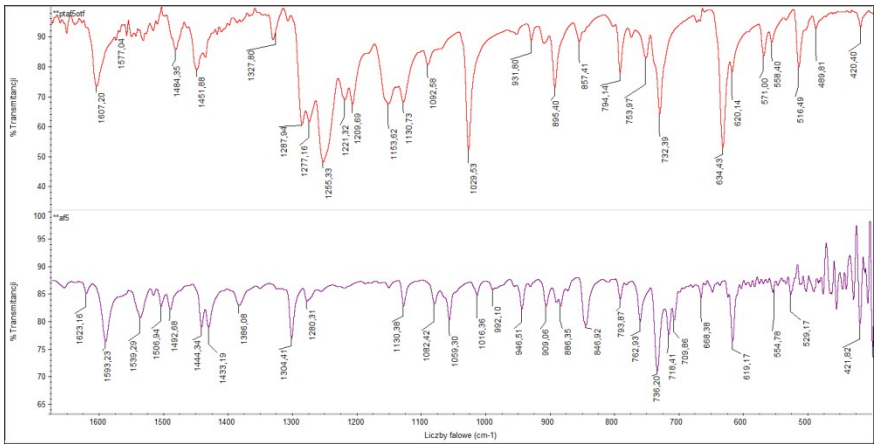

(**1**) and $\mathbf{L^1}$

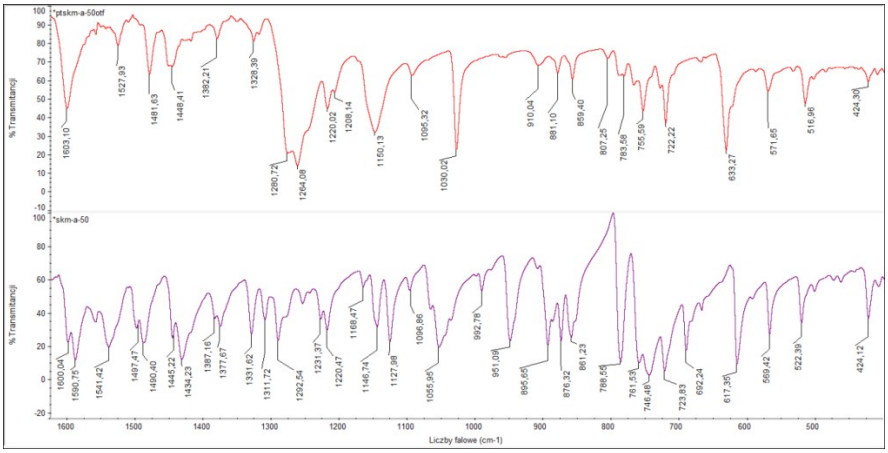

(**2**) and $\mathbf{L^2}$

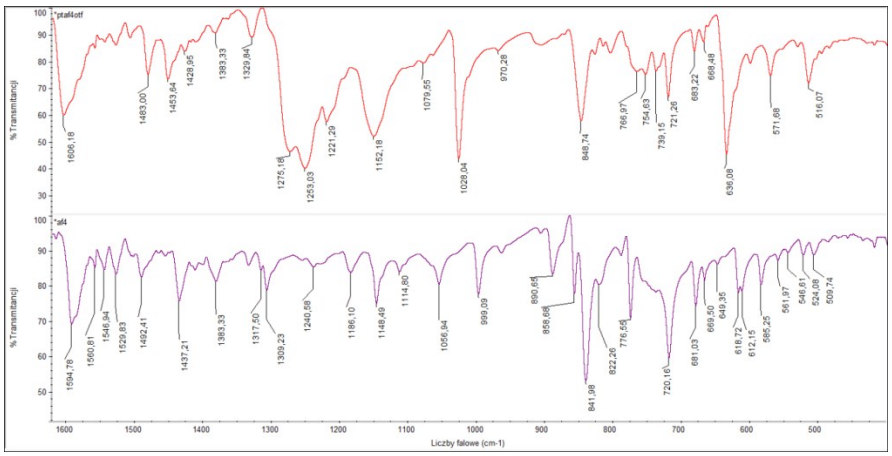

(**3**) and $\mathbf{L^3}$

Figure S1. FT-IR spectra of (**1**)–(**3**) (red) and ligands $\mathbf{L^1}$-$\mathbf{L^3}$ (violet)

^{1}H	^{13}C
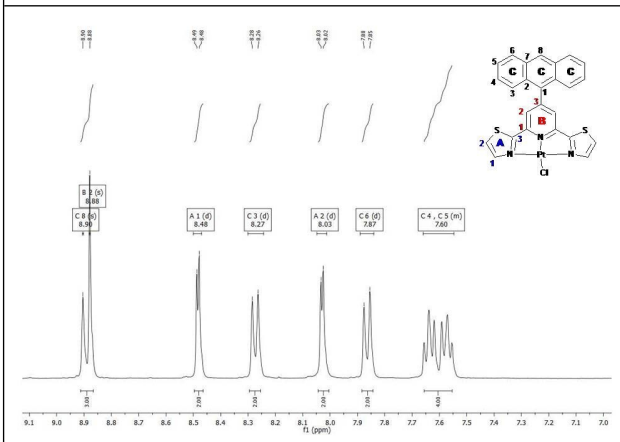	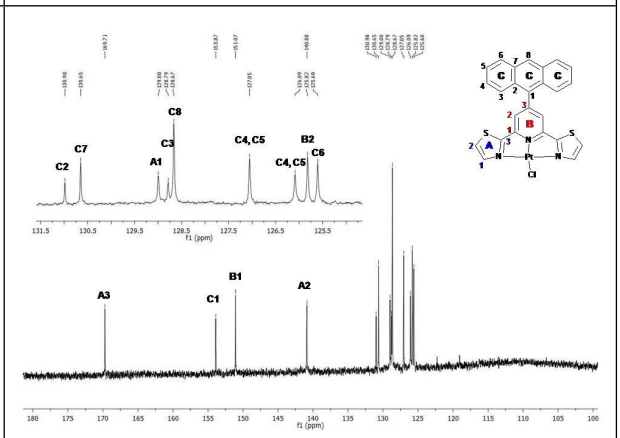
^{1}H-^{13}C HMBC	^{1}H-^{13}C HMQC
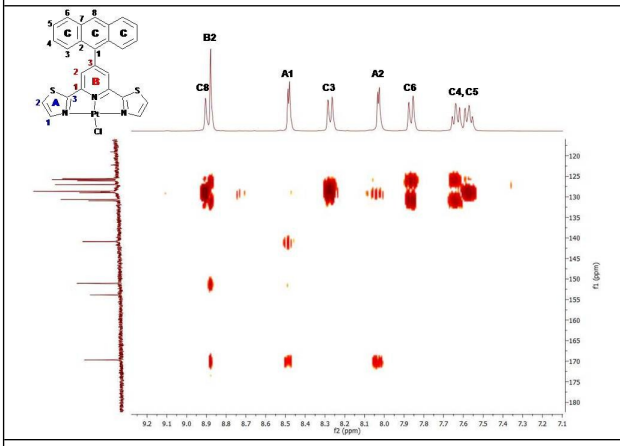	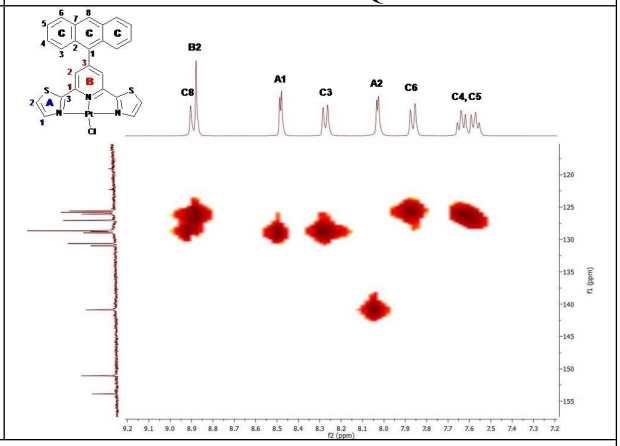
^{1}H-^{1}H COSY	
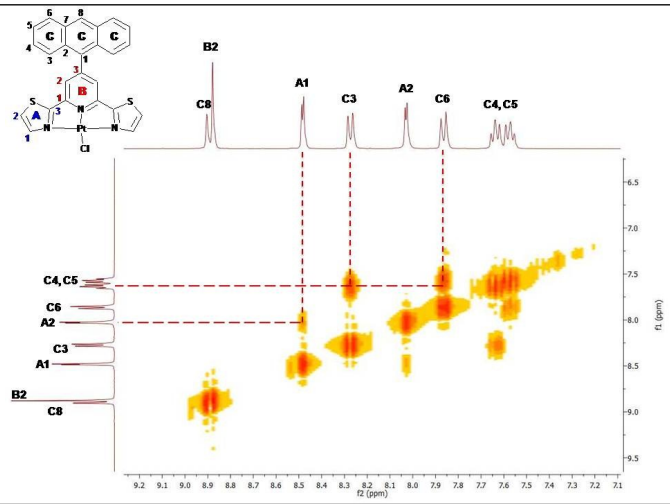	
(1)	

^{1}H	^{13}C
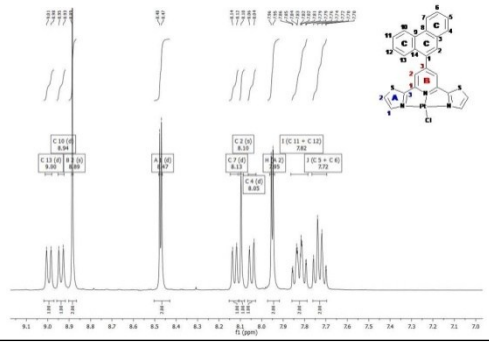	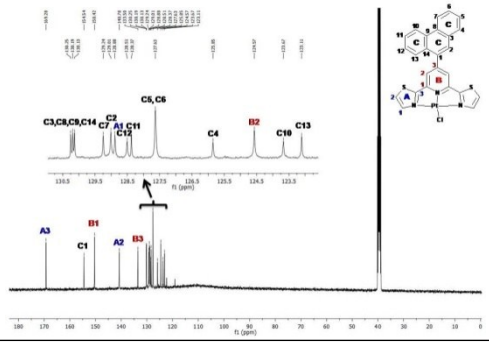
^{1}H-^{13}C HMBC	^{1}H-^{13}C HMQC
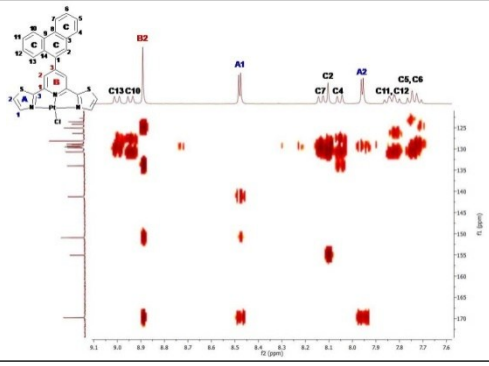	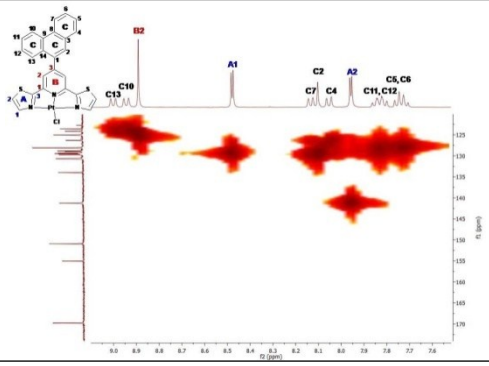
^{1}H-^{1}H COSY	
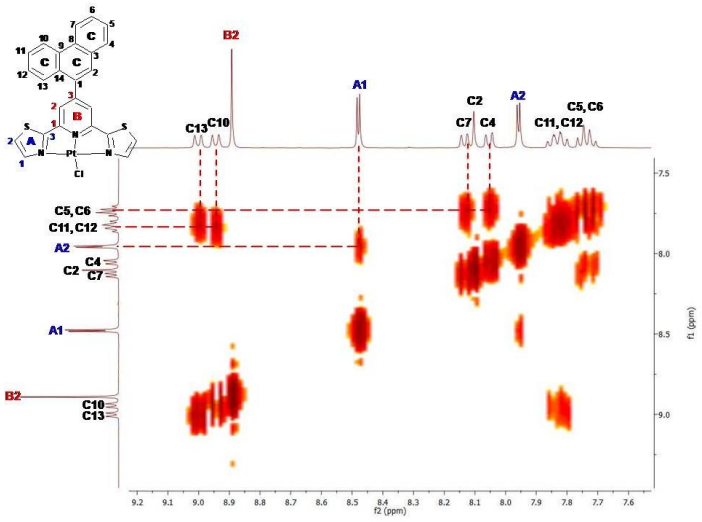	
(2)	

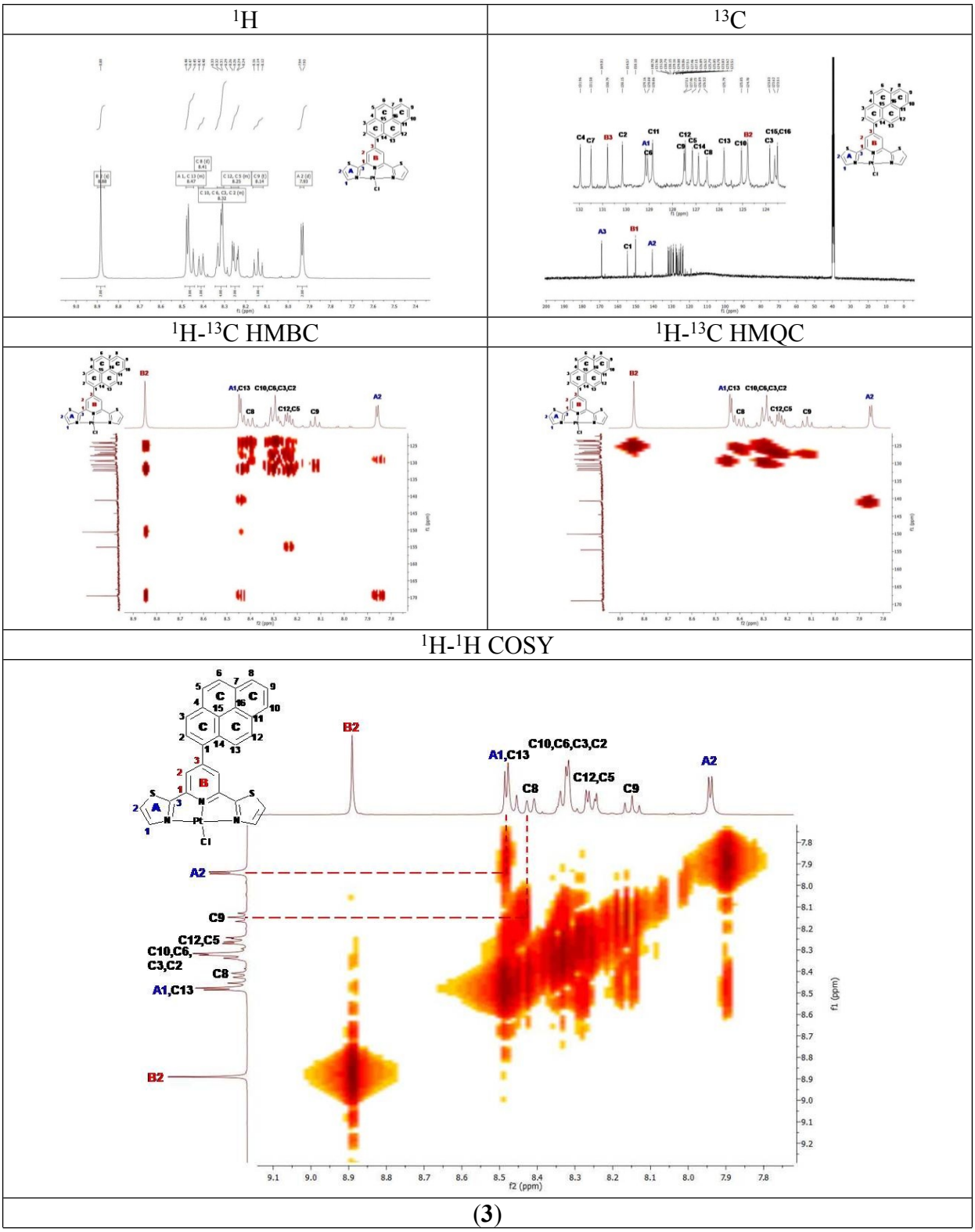

Figure S2. NMR spectra of (**1**)–(**3**)

(**1**)

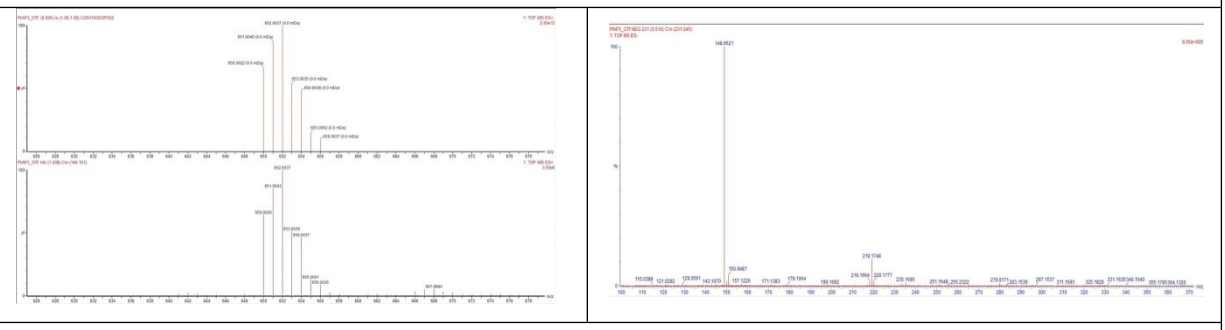

(**2**)

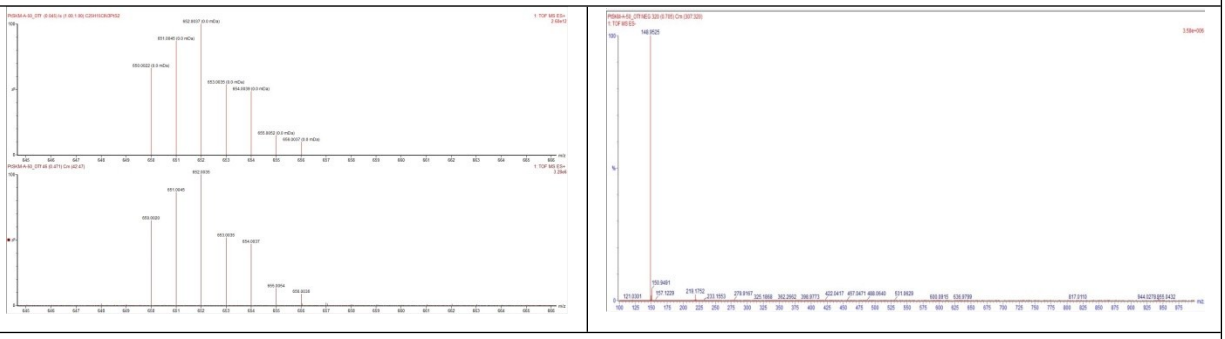

(**3**)

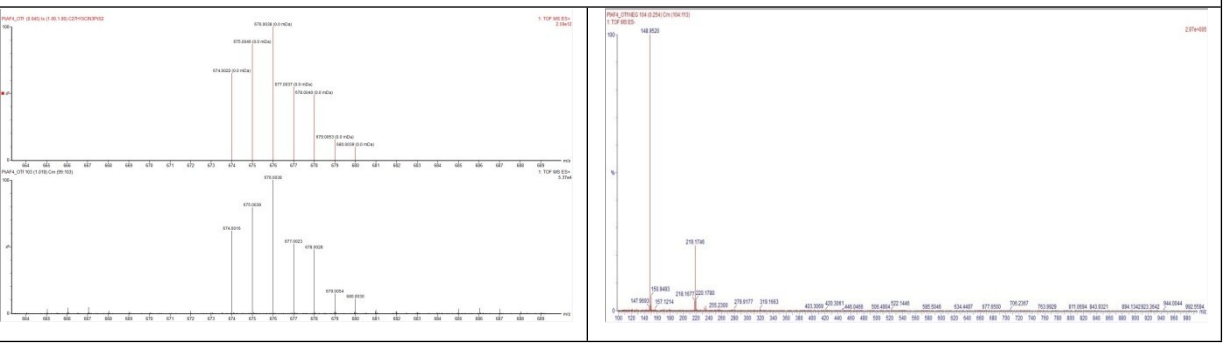

Figure S3. Positive (left) and negative (right) HR-MS spectra of (**1**)–(**3**)

CRYSTALLOGRAPHY

Table S1. Crystallographic data of (**1**)

	(**1**)
Empirical formula	$C_{25}H_{15}S_2N_3ClPt$, CF_3SO_3
Formula weight	801.13
Temperature [K]	295(2)
Crystal system	monoclinic
Space group	$P2_1/c$
Unit cell dimensions	
a [Å]	11.3288(7)
b [Å]	30.4681(12)
c [Å]	7.9355(4)
α [°]	90
β [°]	109.536(6)
γ [°]	90
Volume [Å^3]	2581.4(2)
Z	4
Calculated density [Mg/m^3]	2.061
Absorption coefficient [mm^{-1}]	5.841
F(000)	1544
Crystal dimensions [mm]	0.17×0.12×0.03
θ range for data collection [°]	3.38 – 25.05
Index ranges	$-13 \le h \le 13$,
	$-36 \le k \le 36$,
	$-9 \le l \le 9$
Reflections collected	15850
Independent reflections	4565 [R(int) = 0.0403, R_σ = 0.0388]
Data / restraints / parameters	4565/0/361
Goodness-of-fit on F^2	1.098
Final R indices [I>2σ(I)]	R_1 = 0.0434,
	wR_2= 0.0993
R indices (all data)	R_1 = 0.0541,
	wR_2 = 0.1033
Largest diff. Peak and hole	3.323/-1.324
CCDC	1059808

Table S2. Selected bond lengths [Å] and angles [°] for (**1**)

	(**1**)
Bond length [Å]	
Pt(1)–N(1)	2.003(6)
Pt(1)–N(2)	1.941(6)
Pt(1)–N(3)	2.016(6)
Pt(1)–Cl(1)	2.297(2)
Angle [°]	
N(2)–Pt(1)–N(1)	80.5(2)
N(2)–Pt(1)–N(3)	80.2(2)
N(1)–Pt(1)–N(3)	160.7(2)
N(1)–Pt(1)–Cl(1)	99.53(18)
N(2)–Pt(1)–Cl(1)	179.14(17)
N(3)–Pt(1)–Cl(1)	99.81(18)

Table S3. Hydrogen bonds and stacking interactions in the crystal structure of (**1**)

A. Hydrogen bonds for (**1**)

D-H•••A	d(D–H) [Å]	d(H•••A) [Å]	d(D•••A) [Å]	<(DHA) [°]
(**1**)				
C(2)-H(2) •••O(1)[a]	0.93	2.53	3.050(11)	115.3
C(10)-H(10) •••O(1)[b]	0.93	2.35	3.149(10)	143.5
C(11)-H(11) •••O(2)[b]	0.93	2.42	3.256(10)	150.3

Symmetry codes: (a) -1+x,y,z and (b) x,½-y,-½+z;

B. Short π•••π interactions for (**1**)

Cg(I)•••Cg(J)	Cg(I)•••Cg(J) [Å]	α[°]	β[°]	γ [°]	Cg(I)-Perp [Å]	Cg(J)-Perp [Å]
Cg(6): C(12)-C(13)-C(14)-C(19)-C(20)-C(25)						
Cg(6)•••Cg(6)[a]	3.990(5)	0	17.02	17.02	3.815(4)	3.815(4)

α = dihedral angle between *Cg*(I) and *Cg*(J); *Cg*(I)-Perp = Perpendicular distance of *Cg*(I) on ring J; *Cg*(J)-Perp = perpendicular distance of *Cg*(J) on ring I; β = angle *Cg*(I)→*Cg*(J) vector and normal to ring I; γ = angle *Cg*(I) →*Cg*(J) vector and normal to plane J;
Symmetry codes:(a) 1-x,1-y,2-z;

C. Y—X•••Cg(J) (π-ring) interactions for (**1**)

Y-X(I)•••Cg(J)	X(I)•••Cg(J) [Å]	X-Perp [Å]	γ [°]	Y-X(I)•••Cg(J) [°]
Cg(3): S(1)-C(1)-N(1)-C(3)-C(2); Cg(4): S(2)-C(9)-N(3)-C(11)-C(10)				
Pt(1)-Cl(1)•••Cg(3)[a]	3.537(4)	3.322	20.06	78.38(8)
Pt(1)-Cl(1)•••Cg(4)[b]	3.562(4)	-3.363	19.23	77.09(8)
C(26)-F(2)•••Cg(3)[c]	3.570(9)	-3.405	17.49	115.7(7)
S(3)-O(1)•••Cg(4)	3.650(7)	3.480	17.55	99.1(3)

γ = angle X(I)→Cg(J) vector and normal to plane J.
Symmetry codes: (a) x,½-y,-½+z; (b) x,½-y,½+z; (c) 1+x,y,1+z

D. Ring-metal interactions for (**1**)

Cg(I)•••Me(J)	Cg(I)•••Me(J) [Å]	Me(J)-Perp [Å]	β [°]
Cg(3): S(1)-C(1)-N(1)-C(3)-C(2); Cg(4): S(2)-C(9)-N(3)-C(11)-C(10)			
Cg(3)•••Pt(1)[a]	3.809	3.417	26.21
Cg(4)•••Pt(1)[b]	3.783	-3.358	27.40

Symmetry codes: (a) x,½-y,½+z; (b) x,½-y,-½+z;

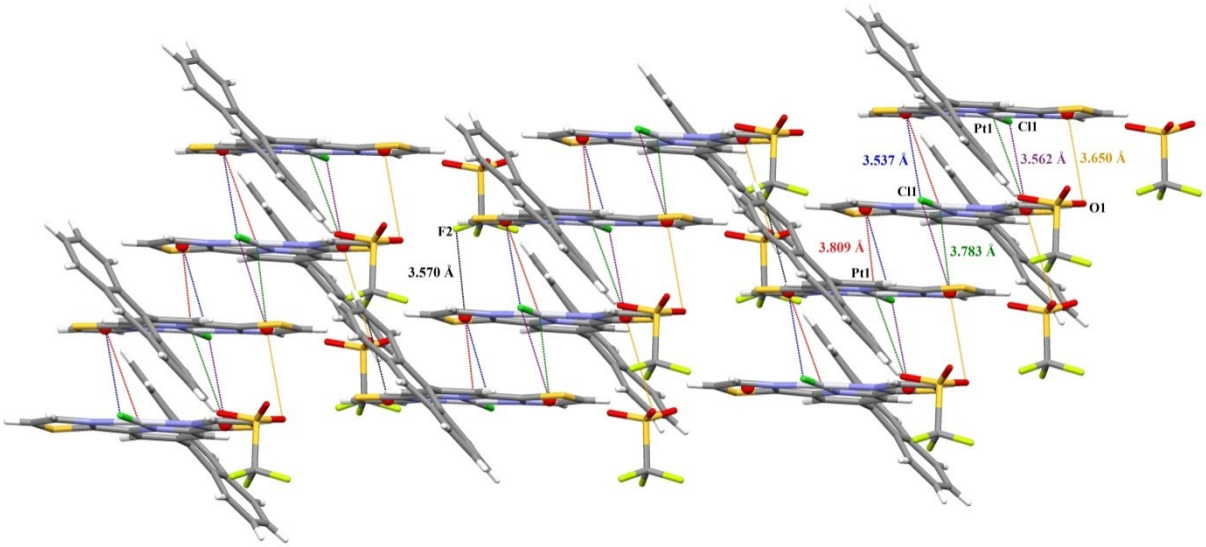

(a)

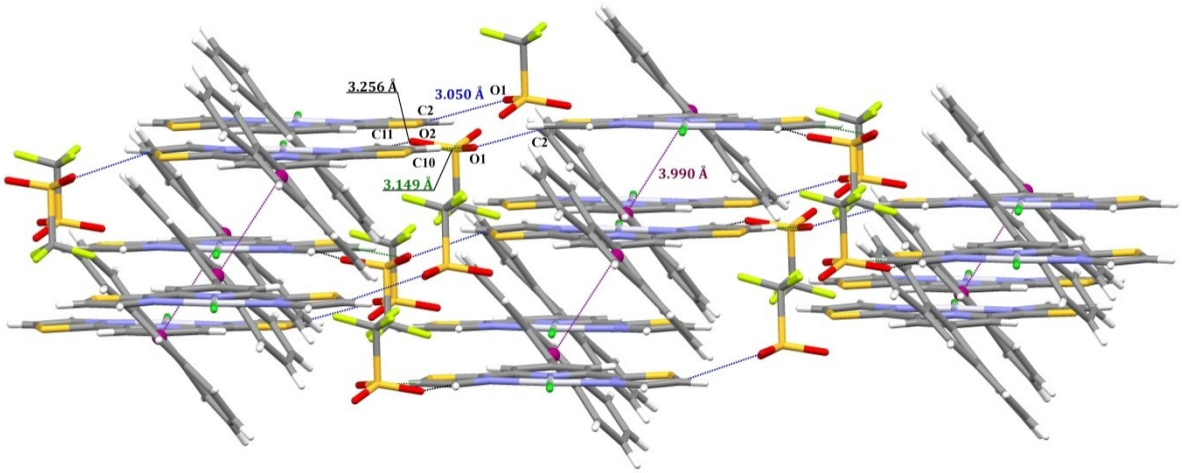

(b)

Figure S4. View of the supramolecular packing of (**1**) showing the (a) Pt•••π, Pt-Cl•••π, C–F•••π, S–O•••π interactions and (b) π•••π interactions, hydrogen bonds of the type C–H•••O.

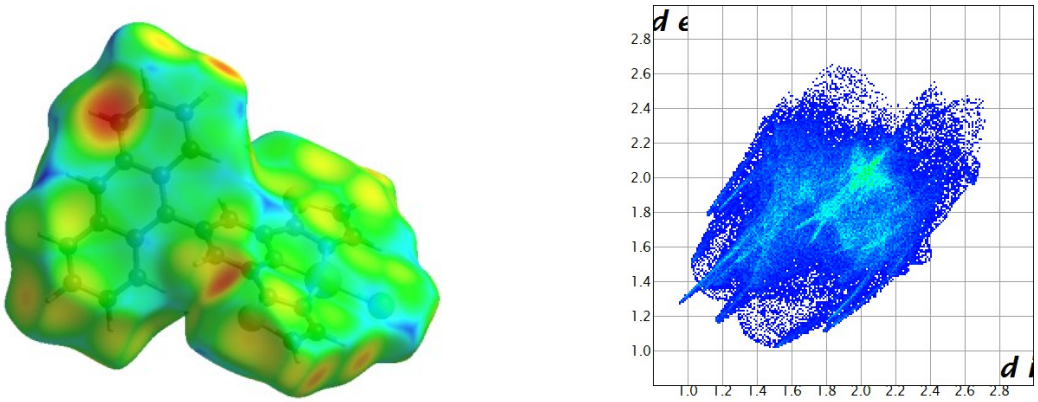

(a) (b)

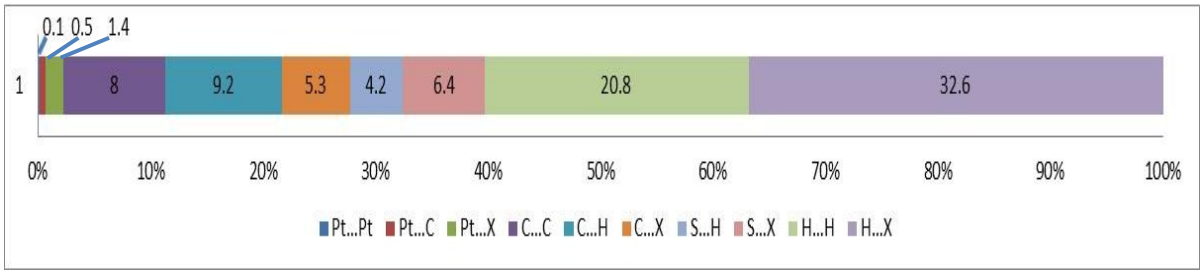

(c)

Figure S5. Hirshfeld surface mapped with d_e (**a**) and 2D fingerprint plots (**b**) for coordination cation of (**1**), along with relative contributions of various intermolecular interactions to the Hirshfeld surfaces (**c**).

Table S4. Structural parameters of phenyl substituted terpyridine platinum(II) coordination compounds [Pt(4′-R-terpy)Cl]X

CSD code (R)	Counter ion	Group	β [°]	α [°]	τ_4'	<$py_{central}$-Ph [°]	Pt-Cl [Å]	Pt-$N_{peripheral}$ [Å]		Pt-$N_{central}$ [Å]	Ref.
Complex 1	$CF_3SO_3^-$	$P2_1/c$	179.14(17)	160.7(2)	0.083	48.58(17)	2.297(2)	2.016(6)	2.003(6)	1.941(6)	—
LAVWUA (H)	$CF_3SO_3^-$	$P2_1/n$	178.9(2)	162.4(3)	0.079	—	2.304(2)	2.015(9)	2.026(8)	1.949(6)	1
JUQVEW (phenyl)	BF_4^-	P-1	179.4(3) 179.8(2)	162.8(4) 161.7(4)	0.073 0.072	24.3(5) 33.4(5)	2.296(3) 2.313(3)	2.008(9) 2.039(9)	2.023(9) 2.013(10)	1.929(10) 1.936(9)	2
ZONJUJ (4-chlorophenyl)	$CF_3SO_3^-$	$P2_1/c$	179.61(12)	161.92(14)	0.074	10.50(15)	2.2994(11)	2.025(4)	2.016(4)	1.930(3)	3
ZONKAQ (4-bromophenyl)	$CF_3SO_3^-$	$P2_1/c$	179.7(3)	161.4(3)	0.075	9.5(3)	2.299(2)	2.017(8)	2.019(8)	1.931(6)	3
OVAREJ (4-bromophenyl)	$B(CF_5)_4^-$	P-1	179.48(5)	161.98(7)	0.075	24.20(7)	2.3003(5)	2.0179(17)	2.0143(16)	1.9352(16)	4
OTULOF (4-methylophenyl)	SbF_6^-	$P2_1/c$	178.72(15)	162.3(2)	0.081	9.1(2)	2.2969(14)	2.027(5)	2.007(5)	1.931(5)	5
IXEBOE (4-methoxyphenyl)	BPh_4^-	P-1	179.01(11)	161.54(17)	0.081	10.4(3)	2.3010(14)	2.015(4)	2.017(4)	1.943(4)	6
ZONJIX [4-(dimethyloamino)phenyl]	BPh_4^-	P-1	178.73(8)	161.74(11)	0.083	14.05(13)	2.3114(10)	2.032(3)	2.018(3)	1.933(3)	7
KUFDOG [4-(diethyloamino)phenyl]	Cl^-	$P2_1/c$	177.98(14)	161.98(18)	0.090	5.08(18)	2.3075(14)	2.011(4)	2.012(4)	1.934(4)	8
DESQEY (4-(dimesitylboryl)phenyl)	PF_6^-	P-1	178.9(1)	162.0(2)	0.081	25.57(18)	2.290(2)	2.017(4)	2.020(4)	1.948(4)	9
LUNLIP (azobenzene)	PF_6^-	P-1	178.7(3)	162.4(4)	0.082	4.6(6)	2.289(11)	2.010(11)	2.01(1)	1.911(13)	10
FAZJOG (p-nicotinamide-N-methylphenyl)	PF_6^-	P-1	179.14(14)	162.13(19)	0.078	51.4(2)	2.3040(16)	2.016(5)	2.021(5)	1.921(5)	11
FAZJUM (p-nicotinamide-N-methylphenyl)	PF_6^-	P-1	179.43(18)	161.9(3)	0.075	43.1(3)	2.306(2)	2.033(6)	2.003(7)	1.933(6)	11
CIZHIE [(3-carbamoyl-)4-pyridinium-1-ylmethylphenyl)	$CF_3SO_3^-$	P-1	178.55(11)	162.24(14)	0.083	34.15(14)	2.2942(11)	2.017(4)	2.020(4)	1.930(3)	12
LABJOO (2-chlorophenyl)	SbF_6^-	$P2_1/n$	179.8(2)	162.1(3)	0.072	54.5(5)	2.303(2)	2.017(7)	2.014(8)	1.941(7)	14

XIPNOZ (2-trifluoromethylphenyl)	SbF_6^-	$P2_1/n$	179.9(3)	162.3(3)	0.069	61.6(4)	2.286(3)	2.014(10)	2.004(10)	1.931(8)	15
XIPNIT (2-methylophenyl)	BF_4^-	$P2_1/n$	179.2(3)	162.3(4)	0.076	68.4(4)	2.293(3)	2.025(11)	2.025(11)	1.935(9)	15
XIPNEP (2-methylophenyl)	SbF_6^-	$Pna2_1$	176.0(12)	161.7(3)	0.112	62.5(9)	2.296(3)	2.027(11)	2.019(9)	1.924(9)	15
ZONJOD (2,4-difluorophenyl)	Cl^-	P-1	179.6(2)	162.1(3)	0.073	40.2(3)	2.284(2)	2.012(8)	2.014(9)	1.944(6)	16
HASMEW (2,4-difluorophenyl)	$CF_3SO_3^-$	P-1	179.4(2)	162.4(3)	0.074	39.4(4)	2.297(2)	2.036(9)	2.003(9)	1.962(7)	17
GEYDOG (4-methoxynaphthalen-1-yl)	$CF_3SO_3^-$	$P2_1/c$	176.71(17)	162.4(2)	0.101	39.79(19)	2.2906(18)	2.006(6)	2.004(6)	1.927(5)	6
REHVUZ (pyren-1-yl)	$B(CF_5)_4^-$	P-1	177.5(3)	161.3(3)	0.099	43.5(2)	—	2.024(7)	2.024(7)	1.984(7)	18
			179.2(3)	159.8(3)	0.086	44.6(2)	—	2.027(7)	2.021(7)	1.983(7)	

Cif files were taken from Cambridge Structural Database 2018

ELECTROCHEMISTRY

Table S5. Electrochemistry of (**1**)–(**3**) compared to $\mathbf{L^1}$–$\mathbf{L^3}$ and [Pt(4′-Ar-terpy)Cl]$^+$ systems

Compound	Medium	E_{red} [V]	E_{ox} [V]	E_{LUMO} [eV][a]	E_{HOMO} [eV][b]	Ref
(1)	CH_3CN	-1.02, -1.48	0.49, 0.92, 1.08	-4.08	-5.59	-
L^1	CH_3CN	-2.13, -2.33	0.85, 1.21	-2.97	-5.95	-
(2)	CH_3CN	-1.00, -1.59, -2.14	0.52, 1.18	-4.10	-5.62	-
L^2	CH_3CN	-2.20	1.23	-2.90	-6.33	-
(3)	CH_3CN	-0.95, -1.56, -1.77	0.43, 0.94	-4.15	-5.43	-
L^3	CH_3CN	-2.07, -2.32	0.86, 1.07	-3.03	-5.96	-
[Pt(4′-phenanthr-9-yl-terpy)Cl]PF_6	DMF	-1.22, -1.76	-	-3.88	-	[20]
[Pt(4′-pyren-1-yl-terpy)Cl]TFPB	DMF	-1.22, -1.74	-	-3.88	-	[20]
[Pt(4′-pyren-1-yl-terpy)Cl]TFPB	DMF	-1.22	-	-3.88	-	[21]

[a]E_{LUMO}= -5.1-E_{red}; [b]E_{HOMO}= -5.1- E_{ox};

TFPB - tetrakis(3,5-bis(trifluoromethyl)phenyl)borate

ELECTRONIC ABSORPTION SPECTRA AND DFT CALCULATIONS

Table S6. The absorption maxima and molar extinction coefficient values for (**1**)– (**3**) and **L**^{1}–**L**^{3} in $(CH_3)_2SO$ solutions ($c = 5 \cdot 10^{-5}\ mol \cdot dm^{-3}$)

Compound	**λ_{abs} [nm] (ε [dm^3·mol^{-1}·cm^{-1}])**
(**1**)	443.2 (5000), 386.9 (18120), 365.6 (28200), 344.4 (31700), 335.3 (31760), 302.0 (39020), 262.3 (48080)
L^{1}	390.2 (12920), 371.4 (14200), 346.2 (17760), 333.8 (22200), 298.1 (29640), 263.9 (44920)
(**2**)	417.4 (12600), 334.0 (33880), 299.6 (54300), 288.7 (47040), 262.4 (64920)
L^{2}	334.5 (sh) (24440), 302.8 (45240), 262.3 (46680)
(**3**)	444.6 (16240), 371.4 (sh) (18560), 363.3 (sh) (28560), 343.1 (78320), 329.4 (66960), 302.0 (55120), 276.7 (70560)
L^{3}	371.0 (sh) (20780), 347.6 (33980), 331.9 (32560), 288.1 (39680)

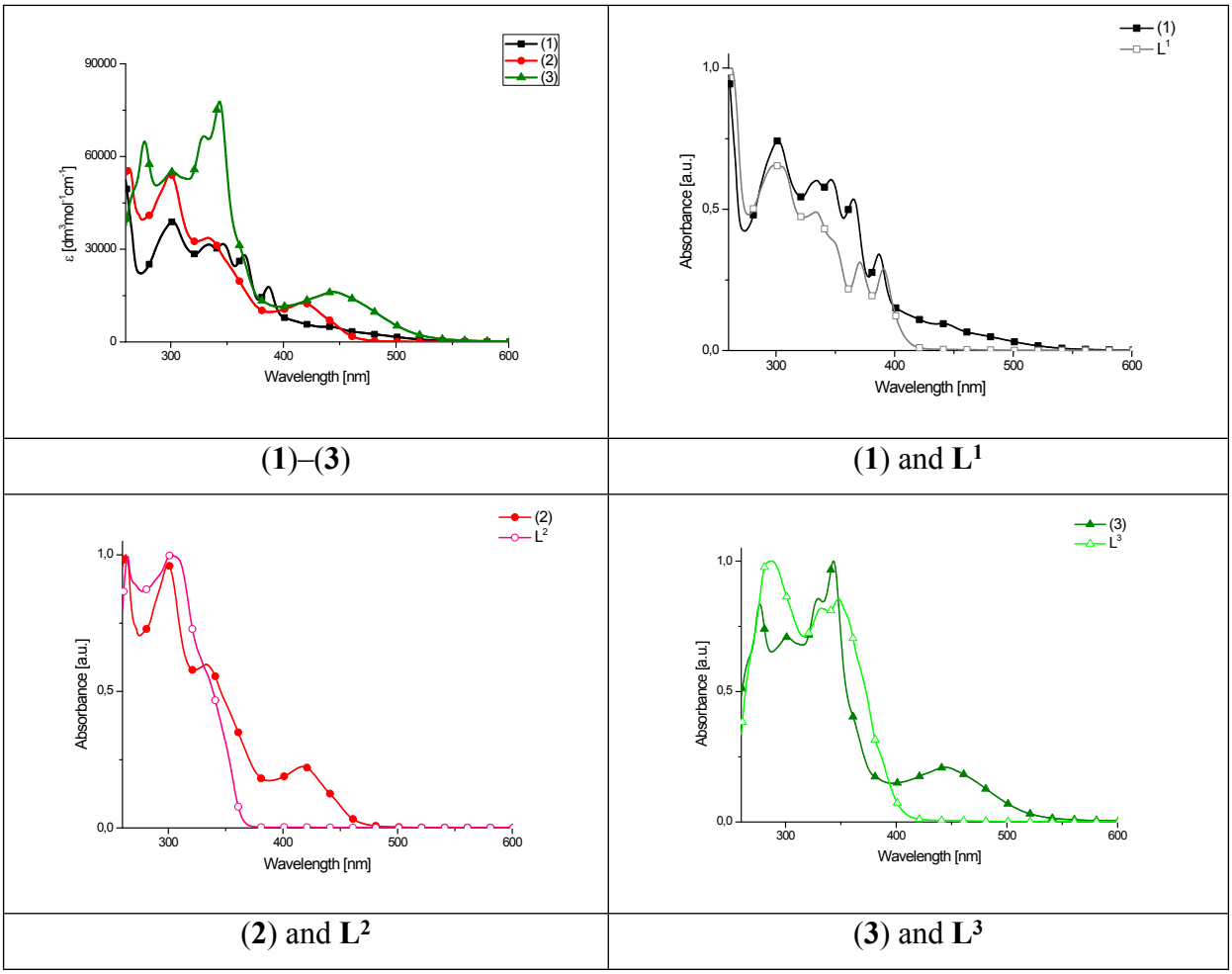

(**1**)–(**3**) | (**1**) and **L**^{1}

(**2**) and **L**^{2} | (**3**) and **L**^{3}

Figure S6. Absorption spectra of (**1**)–(**3**) and **L**^{1}–**L**^{3} in $(CH_3)_2SO$ solutions

Theoretical calculation

The calculations have been performed using the GAUSSIAN-09program package [1]. The geometries of the singlet ground state (S_0) of 1–3 were fully optimized without any symmetry restrictions at the DFT level with the τ-dependent gradient-corrected functional (BMK) [2]. The τ-dependent gradient-corrected functional (BMK) was chosen based on test calculations performed for (**1**) with the use of generalized gradient approximation exchange-correlation (PBE1PBE), conventional hybrid exchange-correlation (B3LYP), long-range corrected (CAM-B3LYP, LC-ωHPBE) functionals, and BMK functional was found to give the best agreement with experimental data (see Fig. S7). The calculations were performed using the def2-TZVP basis set for carbon, nitrogen, sulphur and hydrogen atoms [3–5]. The starting point for geometry optimization was taken from X-ray structure of (1), and all the subsequent calculations were performed based on the optimized geometries. Vibrational frequencies were calculated on the basis of the optimized geometry to verify that each of the geometries is a minimum on the potential energy surface. Furthermore, on the basis of the optimized ground state geometries, the absorption properties in acetonitrile (CH_3CN) media were calculated by TD-DFT at the BMK functional level and with the polarized continuum model (PCM)[6–7].

[1] Frisch MJ, Trucks GW, Schlegel HB, Scuseria GE, Robb MA, Cheeseman JR, Scalmani G, Barone V, Mennucci B, Petersson GA, Nakatsuji H, Caricato M, Li X, Hratchian HP, Izmaylov AF, Bloino J, Zheng G, Sonnenberg JL, Hada M, Ehara M, Toyota K, Fukuda R, Hasegawa J, Ishida M, Nakajima T, Honda Y, Kitao O, Nakai H, Vreven T, Montgomery Jr. JA, Peralta JE, Ogliaro F, Bearpark M, Heyd JJ, Brothers E, Kudin KN, Staroverov VN, Kobayashi R, Normand J, Raghavachari K, Rendell A, Burant JC, Iyengar SS, Tomasi J, Cossi M, Rega N, Millam JM, Klene M, Knox JE, Cross JB, Bakken V, Adamo C, Jaramillo J, Gomperts R, Stratmann RE, Yazyev O, Austin AJ, Cammi R, Pomelli C, Ochterski JW, Martin RL, Morokuma K, Zakrzewski VG, Voth GA, Salvador P, Dannenberg JJ, Dapprich S, Daniels AD, Farkas Ö, Foresman JB, Ortiz JV, Cioslowski J, Fox DJ. Gaussian, Inc., Wallingford CT, 2009.

[2] A.D. Boese, J.M.L. Martin Development of density functionals for thermochemical kinetics J. Chem. Phys., 121 (2004), pp. 3405-3416

[3] Andrae D, Haussermann U, Dolg M, Stoll H, Preuss H. Energy-adjusted ab initio pseudopotentials for the second and third row transition elements. Theor Chim Acta 1990, 77: 123–141.

[4] Weigend F, Ahlrichs R. Balanced basis sets of split valence, triple zeta valence and quadruple zeta valence quality for H to Rn: design and assessment of accuracy. Phys Chem Chem Phys 2005, 7: 3297–3305.

[5] Weigend F. Accurate Coulomb-fitting basis sets for H to Rn. Phys Chem Chem Phys 2006, 8: 1057–1065.

[6] Mennucci B, Tomasi J. Continuum solvation models: a new approach to the problem of solute's charge distribution and cavity boundaries. J Chem Phys 1997, 106: 5151–5158.

[7] Cances MT, Mennucci B, Tomasi J. A new integral equation formalism for the Polarizable Continuum Model: theoretical background and applications to isotropic and anisotropic dielectrics. J Chem Phys 1997, 107: 3032–3041.

[8] Cossi M, Barone V, Mennucci B, Tomasi J. Ab initio study of ionic solutions by a Polarizable Continuum Dielectric Model. Chem Phys Lett 1998, 286: 253–260.

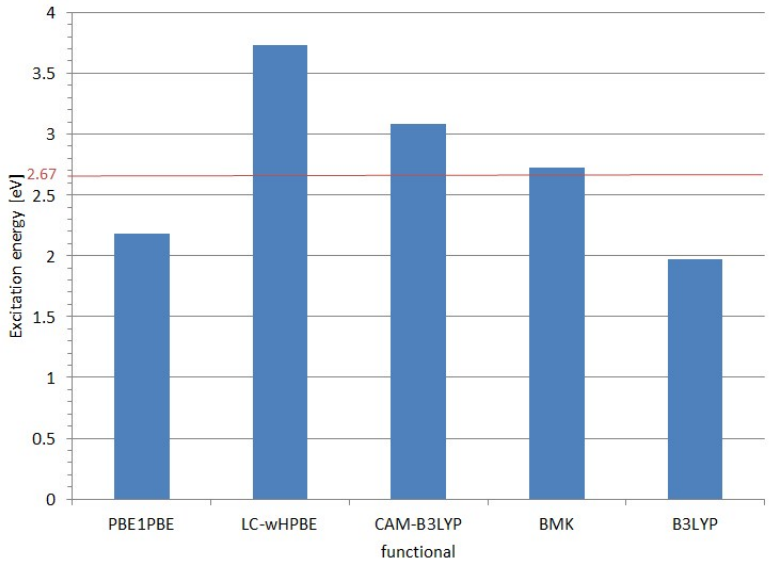

Figure S7. TD-DFT values of excitations energy for excited electronic state of (**1**). The energy (2.67 eV) corresponds to the maximum of lowest band in the experimental absorption

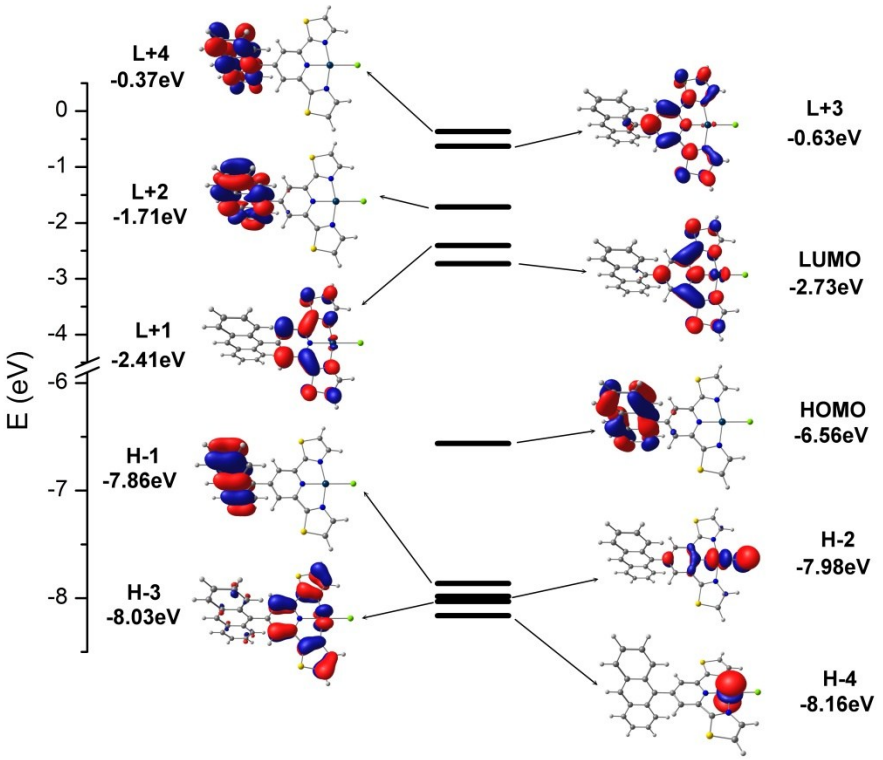
L+4
-0.37eV
L+2
-1.71eV
L+1
-2.41eV
H-1
-7.86eV
H-3
-8.03eV
E (eV)
0
-1
-2
-3
-4
-6
-7
-8
L+3
-0.63eV
LUMO
-2.73eV
HOMO
-6.56eV
H-2
-7.98eV
H-4
-8.16eV

(**1**)

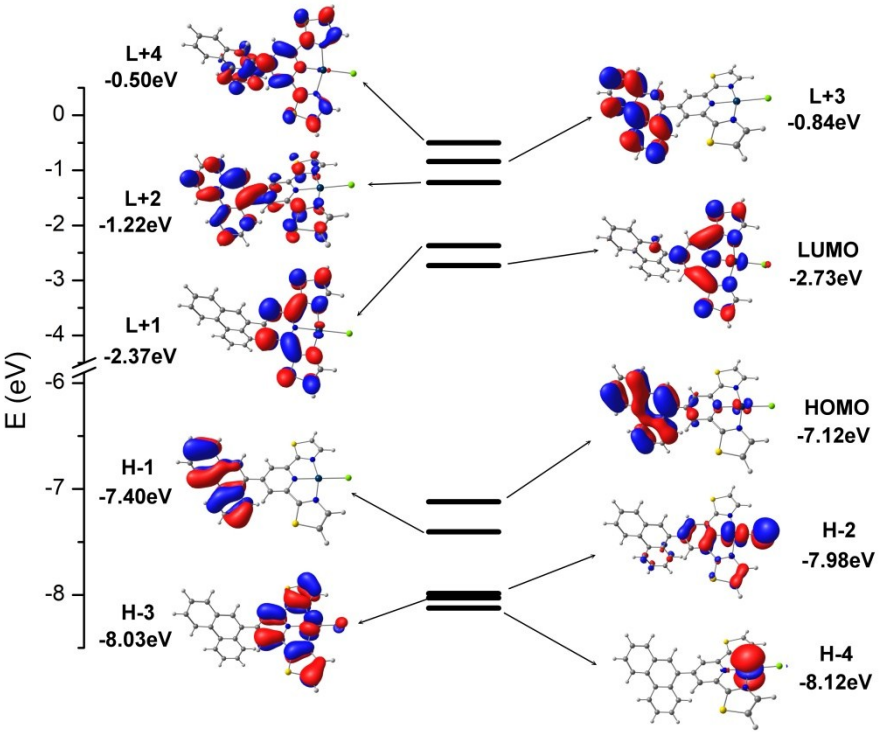
L+4
-0.50eV
L+2
-1.22eV
L+1
-2.37eV
H-1
-7.40eV
H-3
-8.03eV
E (eV)
0
-1
-2
-3
-4
-6
-7
-8
L+3
-0.84eV
LUMO
-2.73eV
HOMO
-7.12eV
H-2
-7.98eV
H-4
-8.12eV

(**2**)

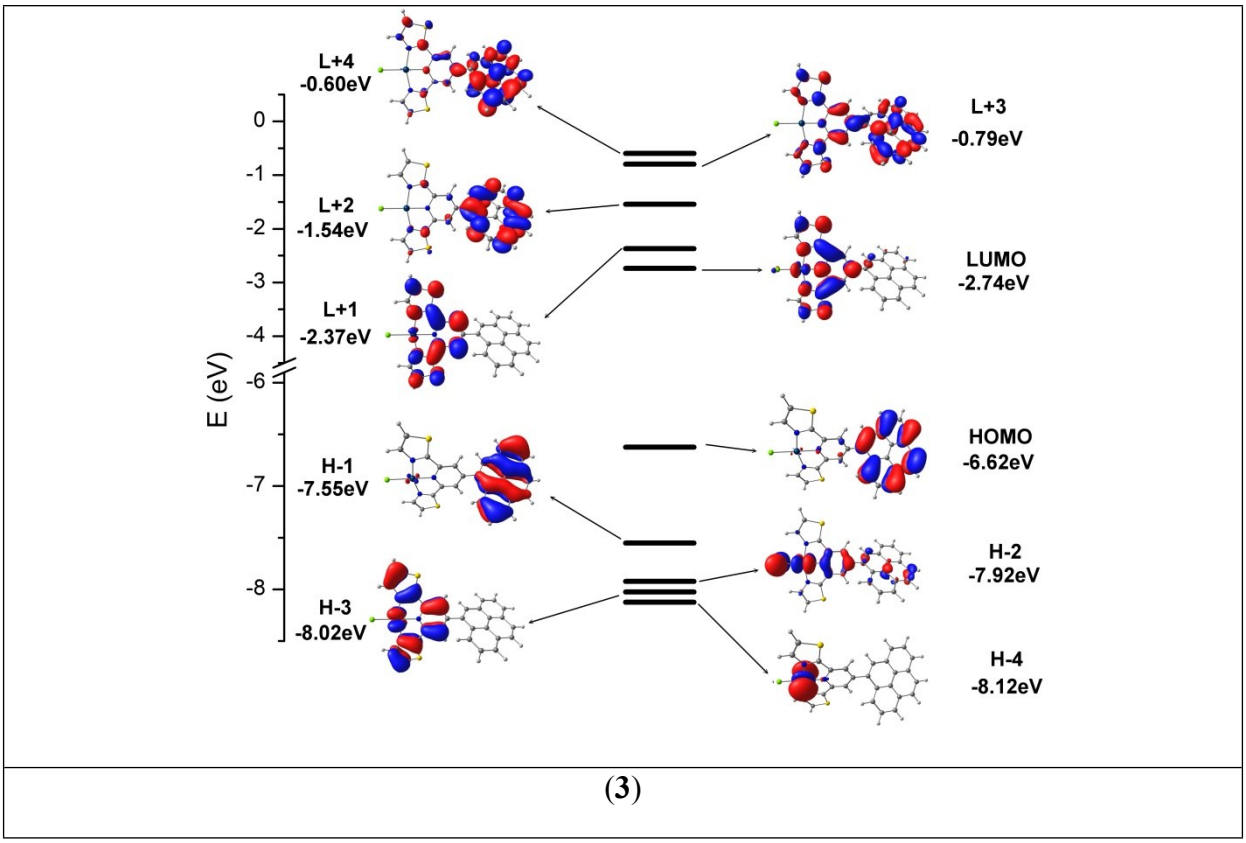

(**3**)

Figure S8. Graphical representations of selected MOs and their TD-DFT energies

Table S7. The energies and characters of the selected spin-allowed electronic transitions for (**1**) calculated with the TDDFT/Def2-TZVPD/BMK method, together with assignment to the experimental absorption bands

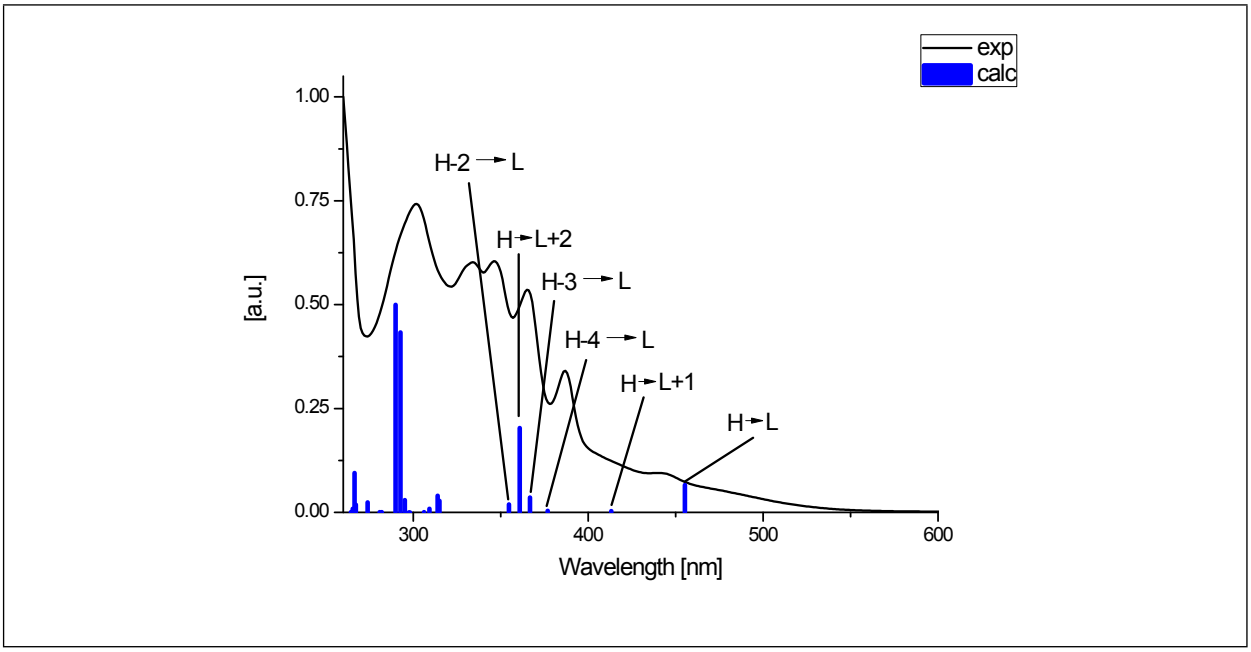

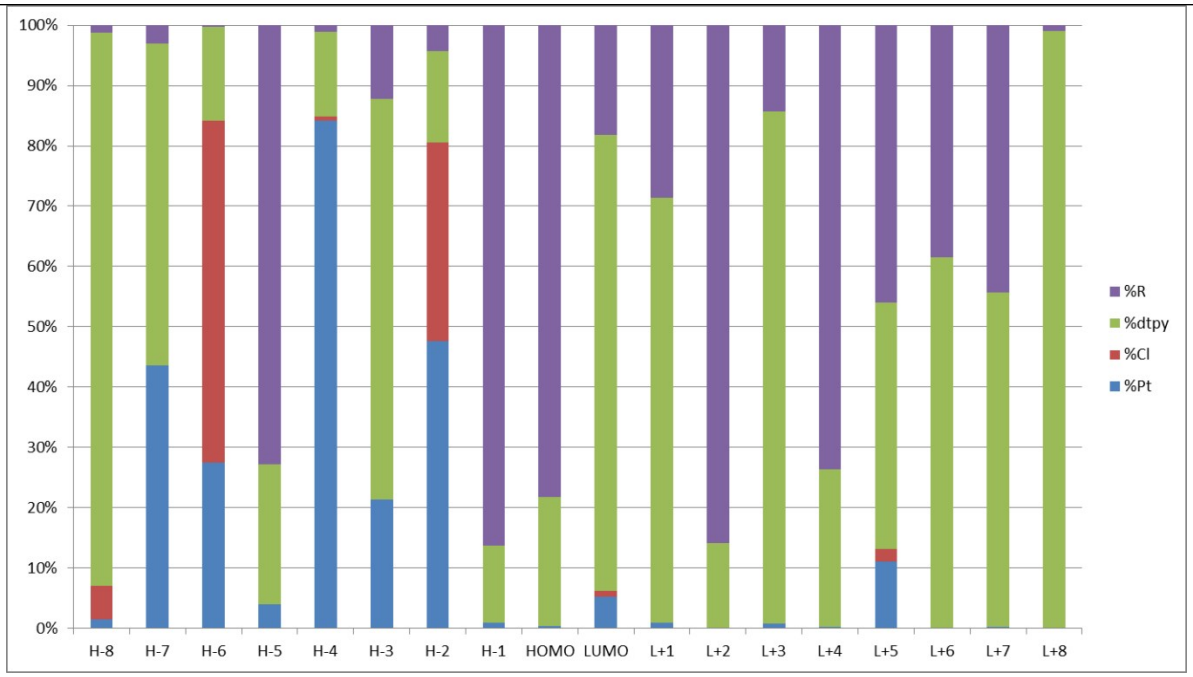

Experimental absorption λ [nm] (10^3 ε [M^{-1} cm^{-1}])/ E [eV]	Calculated transitions			
	Major contribution	λ [nm]/ E [eV]	Character	Oscillator strength
443.2 (5.0)/2.80	HOMO→LUMO (97%)	455.3/2.73	ILCT/LC	0.066
	HOMO→L+1 (98%)	413.2/3.00	ILCT/LC	0.0031
386.9 (18.1)/3.21	H-4→LUMO (98%)	376.9/3.29	MLCT	0.0038
365.6 (28.2)/3.39	H-3→LUMO (83%)	366.7/3.38	LC	0.0354
344.4 (31.7)/3.60	HOMO→L+2 (96%)	360.9/3.44	LC	0.2032
335.3 (31.8)/3.70	H-2→L+1 (89%)	313.9/3.95	MLCT/LC	0.0399
302.0 (39.0)/4.11	H-7→LUMO (80%)	289.9/4.28	LC/ILCT	0.4995

Table S8. The energies and characters of the selected spin-allowed electronic transitions for (**2**) calculated with the TDDFT/Def2-TZVPD/BMK method, together with assignment to the experimental absorption bands

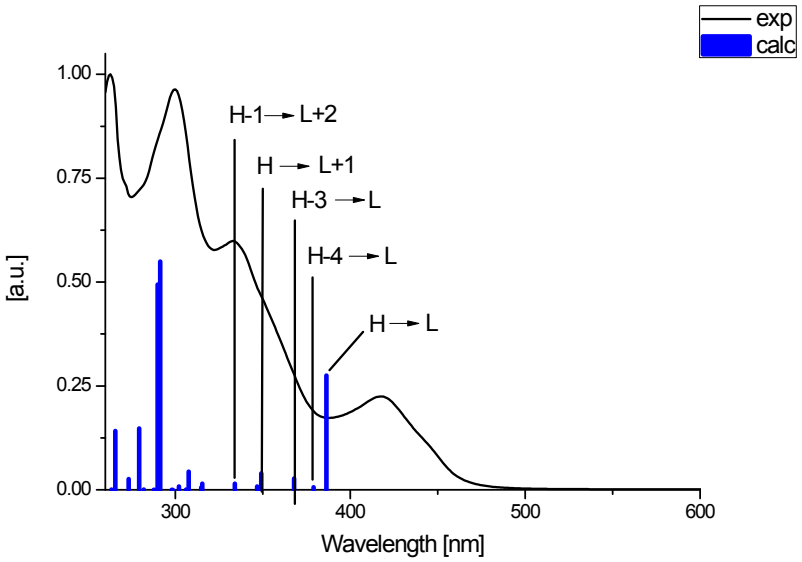

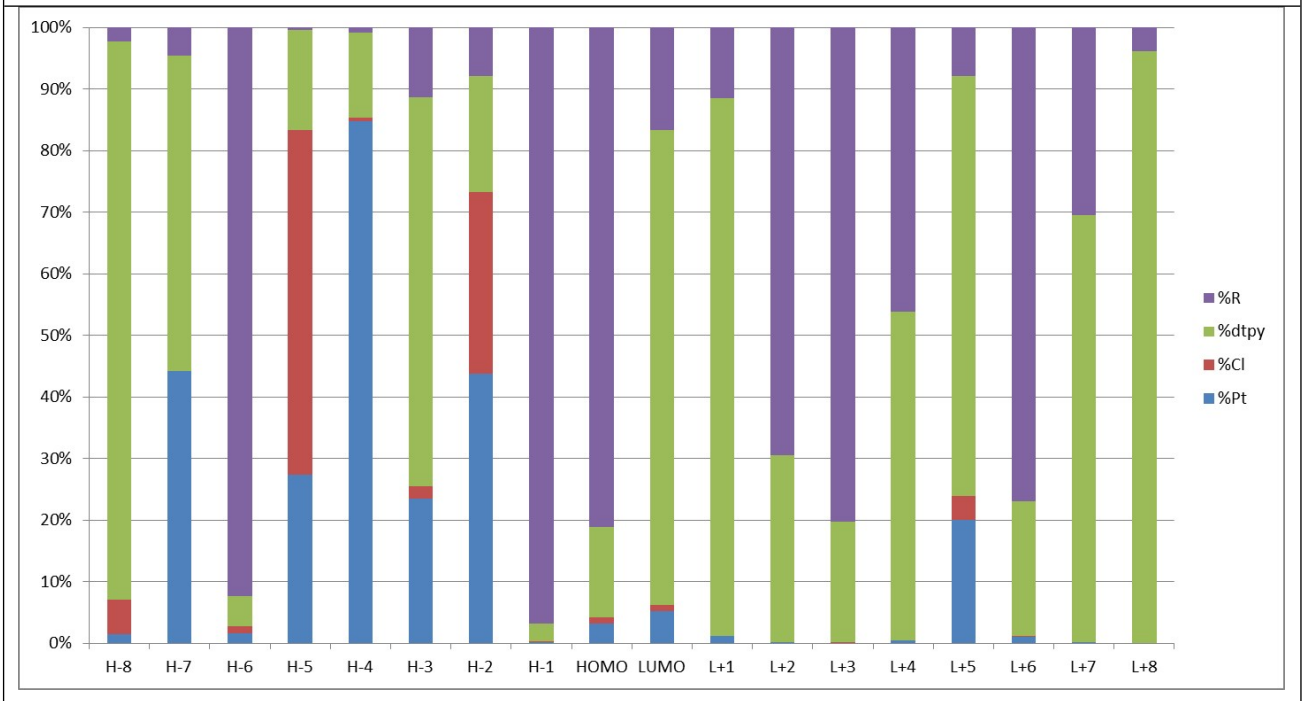

Experimental absorption λ [nm] (10^3 ε [M^{-1} cm^{-1}])/	Calculated transitions			
	Major contribution	λ [nm]/E [eV]	Character	Oscillator strength

E [eV]				
417.4 (12.6)/2.97	HOMO→LUMO (83%)	386.4/3.21	ILCT/LC/MLCT	0.2751
	H-4→LUMO (97%)	379.1/3.27	MLCT	0.0059
	H-3→LUMO (72%), H-3→LUMO (12%)	367.9/3.37	LC/MLCT	0.0273
334.0 (33.9)/3.72	HOMO→L+1 (74%)	349.2/3.55	ILCT/LC/MLCT	0.0395
	H-2→LUMO (53%), HOMO→LUMO (10%), HOMO→L+1 (11%)	346.8/3.58	MLCT/XLCT	0.0077
	H-1→L+2 (90%)	334.0/3.72	LC	0.0148
299.6 (54.3)/4.14	H-3→L+1 (75%)	291.4/4.26	LC	0.5495

Table S9. The energies and characters of the selected spin-allowed electronic transitions for (**3**) calculated with the TDDFT/Def2-TZVPD/BMK method, together with assignment to the experimental absorption bands

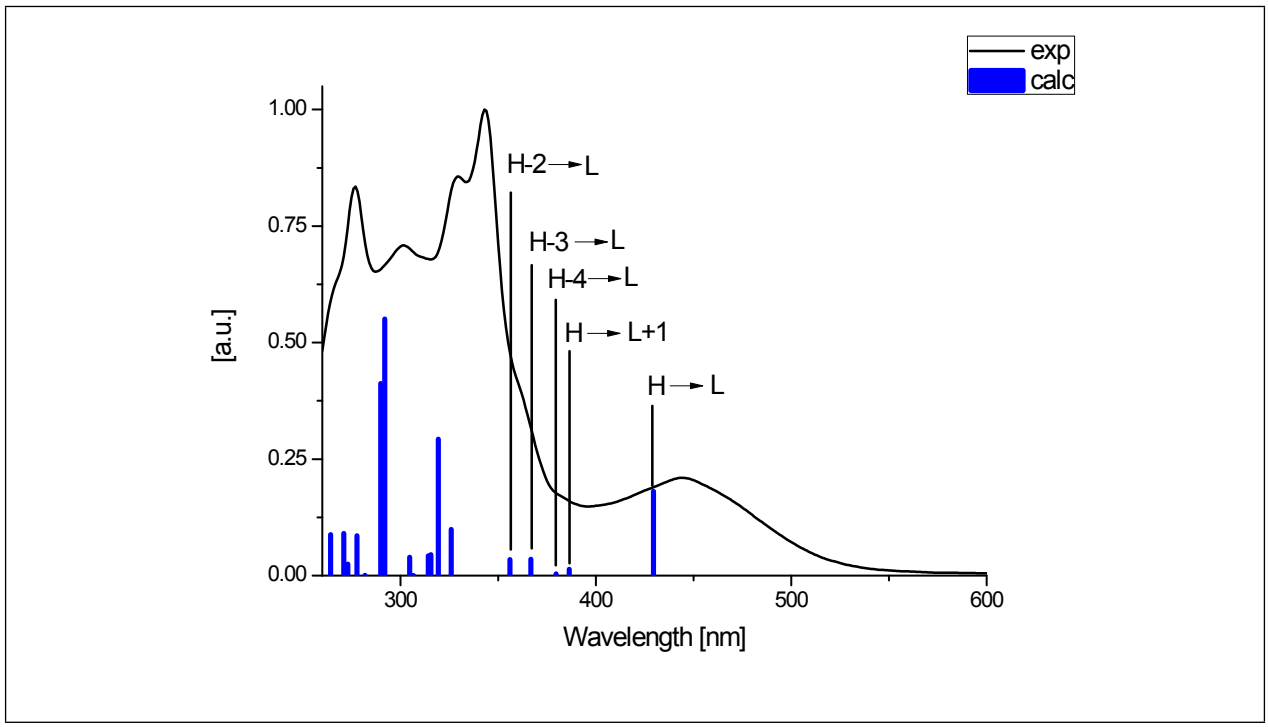

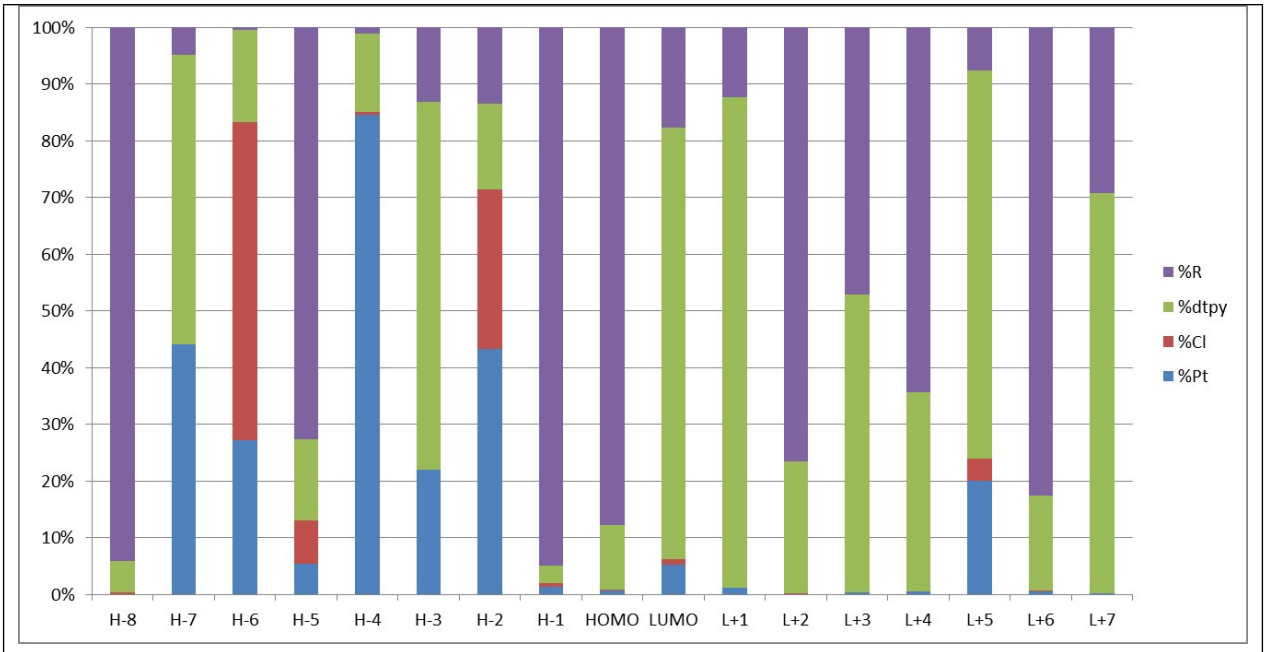

Experimental absorption λ [nm] (10^3 ε [M^{-1} cm^{-1}])/ E [eV]	Calculated transitions			
	Major contribution	λ [nm]/ E [eV]	Character	Oscillator strength
444.6 (16.2)/2.79	HOMO→LUMO (95%)	429.5/2.89	ILCT/LC	0.1807
	HOMO→L+1 (92%)	386.3/3.21	ILCT	0.0136
371.4 (sh) (18.6)/ 3.34	H-4→LUMO (98%)	379.6/3.27	MLCT	0.0039
363.3 (sh) (28.6)/ 3.42	H-3→LUMO (87%)	366.7/3.38	MLCT/LC	0.0353
343.1 (78.3)/3.62	H-2→LUMO (70%)	356/3.48	MLCT/XLCT	0.0347
329.4 (67.0)/3.77	HOMO→L+2 (79%)	319.4/3.88	LC	0.2929
302.0 (55.1)/4.11	H-3→L+1 (78%)	291.9/4.25	LC	0.5508

PHOTOLUMINESCENCE PROPERTIES

Table S10. Photoluminescence properties of complexes (**1**)–(**3**)

Compound	Condition [K]	λ_{exc} [nm]	λ_{em} [nm]	ΔE_{exc-em} [cm^{-1}]	Φ_{em} [%]	τ	χ^2
(**1**)	298	427 (sh), 398, 378, 273	512	3888	6.30	13.45ns (84.57%), 2.92ns (11.72%), 0.03ns (3.71%)	1.097
(**2**)	298	362, 314, 293, 271	472	6438	3.87	6.62ns (6.15%), 2.30ns (45.58%), 0.62ns (48.27%)	0.805
(**3**)	298	444	570	4978	12.16	3.39ns (100%)	1.089

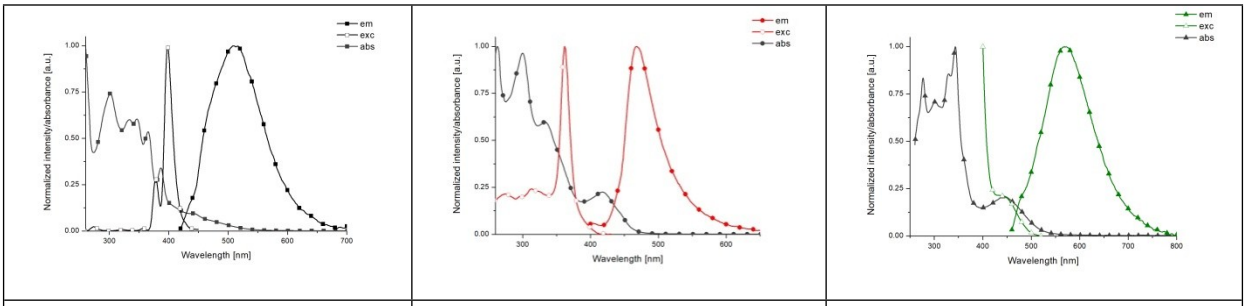

(**1**) (**2**) (**3**)

Figure S9. Absorption, excitation and emission spectra of (**1**)–(**3**) in $(CH_3)_2SO$ solutions

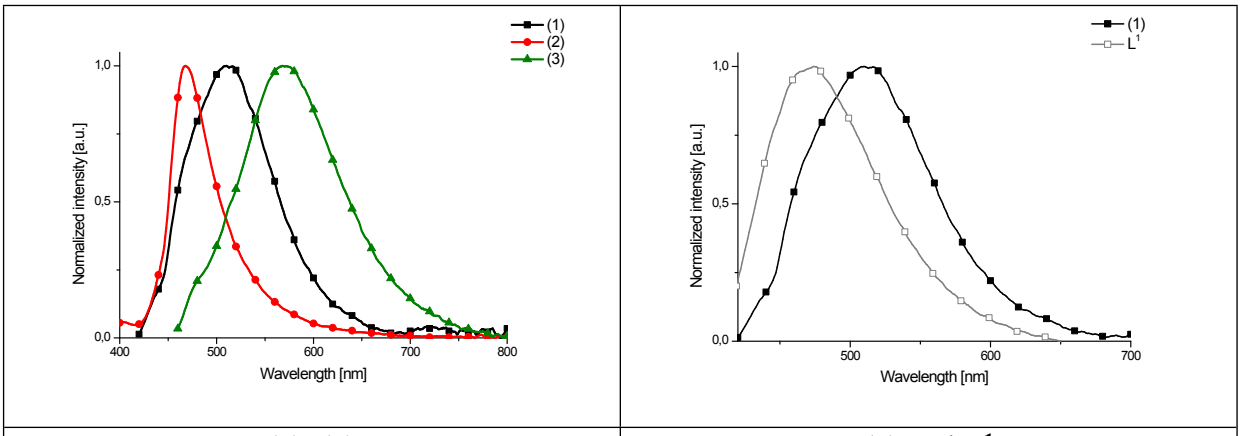

(**1**)–(**3**) (**1**) and **L**[1]

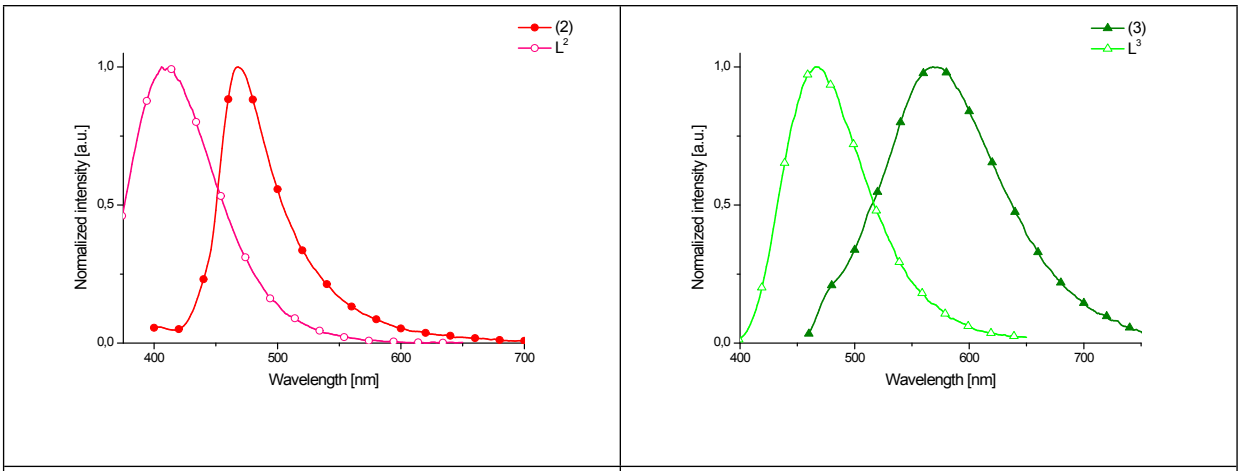

(**2**) and $\mathbf{L^2}$	(**3**) and $\mathbf{L^3}$

Figure S10. Emission spectra of (**1**)–(**3**) and $\mathbf{L^1}$-$\mathbf{L^3}$ in $(CH_3)_2SO$ solutions

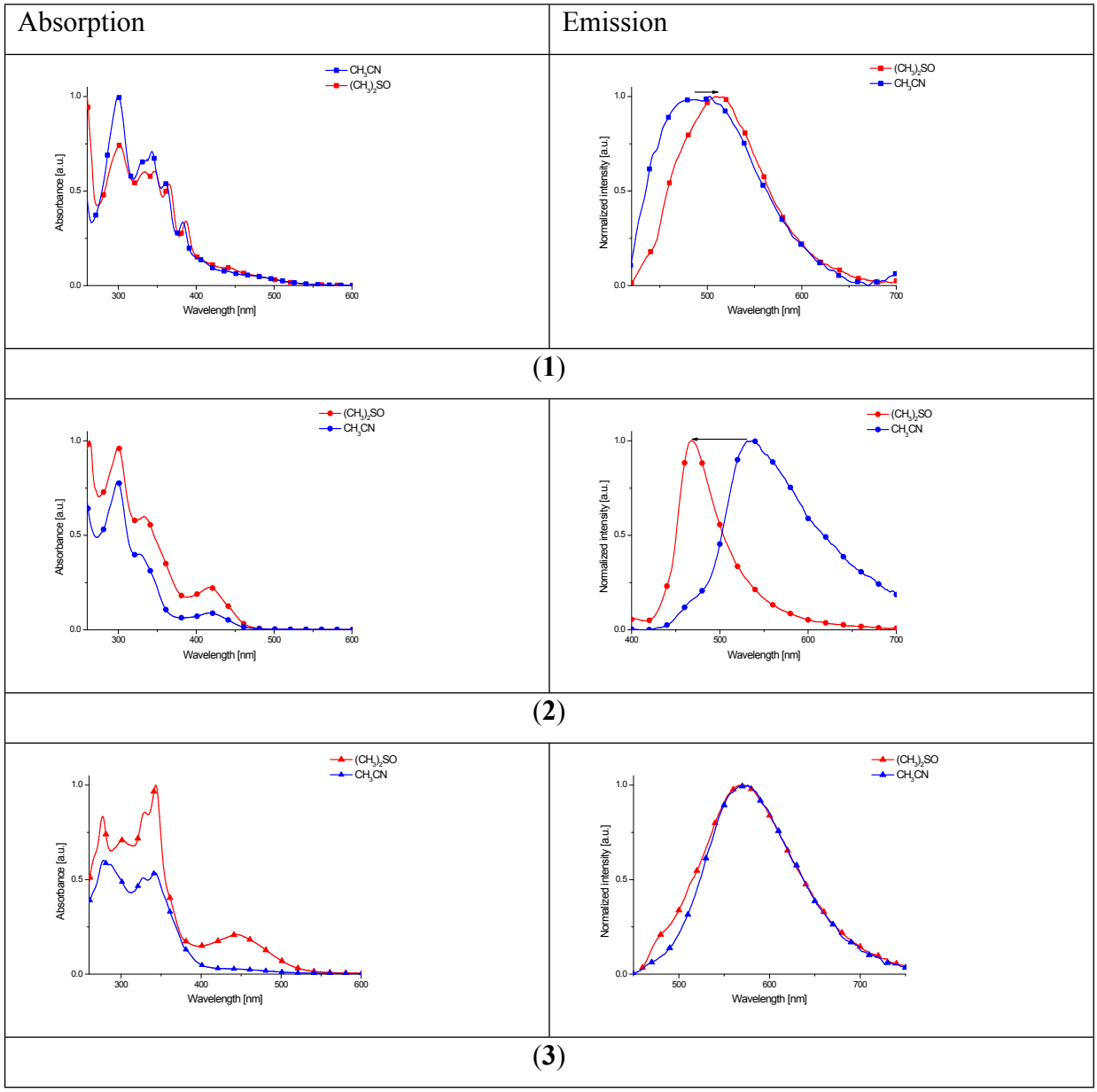

Figure S11. Comparison of electronic spectra of (**1**)–(**3**) in $(CH_3)_2SO$ and CH_3CN solutions

Table S11. Absorption and emission properties of (**1**)–(**3**) compared to $\mathbf{L^1}$–$\mathbf{L^3}$ and [Pt(4′-Ar-terpy)Cl]$^+$

Compound	**Medium**	**λabs (ε [$M^{-1}cm^{-1}$])**	**λem [nm]** **τ; Φ [0-1]; $k_{r/nr}$ [s^{-1}]**	**Ref**
(1)	$(CH_3)_2SO_3$	443 (5000), 387 (18120), 366 (28200), 344 (31700), 335 (31760), 302 (39020), 262 (48080)	512 τ – 11.71ns; Φ -0.0630 k_r – $5.38 \cdot 10^6$; k_{nr} – $80{,}02 \cdot 10^6$	—
	CH_3CN	436 (3320), 406 (4400), 383 (15920), 360 (25240), 345 (32480), 320 (31160), 300 (46720)	488	—
L^1	$(CH_3)_2SO_3$	390.2 (12920), 371.4 (14200), 346.2 (17760), 333.8 (22200), 298.1 (29640), 263.9 (44920)	472 τ – 2.52ns; Φ -0.2136	—
(2)	$(CH_3)_2SO_3$	417.4 (12600), 334.0 (33880), 299.6 (54300), 288.7 (47040), 262.4 (64920)	472 τ -1.76 ns; Φ -0.0387 k_r – $21.98 \cdot 10^6$; k_{nr} – $546{,}20 \cdot 10^6$	—
	CH_3CN	420 (6760), 332 (29360), 299 (59160)	466, 535	—
L^2	$(CH_3)_2SO_3$	334.5 (sh) (24440), 302.8 (45240), 262.3 (46680)	410 τ – 1.75ns; Φ -0.3124	—
(3)	$(CH_3)_2SO_3$	444.6 (16240), 371.4 (sh) (18560), 363.3 (sh) (28560), 343.1 (78320), 329.4 (66960), 302.0 (55120), 276.7 (70560)	570 τ – 3.39ns; Φ -0.1216 k_r – $35.87 \cdot 10^6$; k_{nr} – $259.12 \cdot 10^6$	—
	CH_3CN	456 (1440), 382 (6640), 342 (28440), 327 (26760), 286 (30560), 278 (31720), 265 (22720)	569	—
L^3	$(CH_3)_2SO_3$	371.0 (sh) (20780), 347.6 (33980), 331.9 (32560), 288.1 (39680)	467 τ – 3.32ns; Φ -0.6269	—
[Pt(4′-anthr-9-yl-terpy)Cl]PF_6	CH_3CN	447 (2600), 383 (10990), 363 (11500), 347 (15810), 332 (19600), 319 (13460), 304 (12710), 284 (36580), 276 (28430), 253 (178840)	600, 712 Φ - 0.0002	[19]
[Pt(4′-phenanthr-9-yl-terpy)Cl]PF_6	CH_3CN	409 (7670), 334 (16780), 320 (14680), 296 (24250), 284 (46500), 254 (73210),	582 τ - 202ns; Φ -0.0016 k_r – $7.9 \cdot 10^3$; k_{nr} – $4.94 \cdot 10^6$	[19]
[Pt(4′-phenanthr-9-yl-terpy)Cl]PF_6	CH_2Cl_2	429, 385sh, 335, 322sh, 296sh, 285	610 τ - 21μs; Φ - 0.070	[20]
[Pt(4′-pyren-1-yl-terpy)Cl]PF_6	CH_3CN	438 (10330), 380 (5990), 338 (37780), 327 (33690), 310 (22130), 283 (48640), 275 (46340), 263 (39930)	658 Φ - 0.0013	[19]

[Pt(4′-pyren-1-yl-terpy)Cl]TFPB	CH_2Cl_2	476 (8910), 405, 387, 340, 328sh, 310sh	700; τ-64μs; Φ – 0.034	[21]
[Pt(4′-pyren-1-yl-terpy)Cl]TFPB	CH_2Cl_2	476, 405, 387, 340, 329sh, 310sh, 284	650 τ - 1ns; Φ - 0.001 k_r – $1.0 \cdot 10^6$; k_{nr} – $999.0 \cdot 10^6$ 700 τ - 64μs; Φ - 0.034 k_r – $0.53 \cdot 10^3$; k_{nr} – $0.966 \cdot 10^6$	[20]

TFPB - tetrakis(3,5-bis(trifluoromethyl)phenyl)borate

CYTOTOXIC ACTIVITY

Table S12. Summary of the cytotoxic properties of [Pt(4′-R-terpy)Cl]X and transition metal coordination compounds of *dtpy*

Compound	Cell line	IC_{50} (μM)	Ref.
$[Pt(terpy)Cl]BF_4$	CH1 $CH1cis^R$ $CH1dox^R$ A2780 $A2780cis^R$ SKOV3	6.6 6.4 3.75 49 41 19.5	[33]
[Pt(terpy)Cl]Cl	MCF-7	25	[34]
[Pt(4′-phenyl-terpy)Cl]Cl	HaCaT (light) HaCaT (dark) MCF-7 (light) MCF-7 (dark)	1.6 ± 0.2 4.8 ± 0.6 3.6 ± 0.1 7.4 ± 0.5	[35]
{Pt[4′-(4-methoxyphenyl)-terpy]Cl}Cl	HL-60 BGC-823 KB Bel-7402	13.09±1.27 9.93±0.52 6.71±0.38 3.66±0.14	[36]
$\{Pt[4'-(4\text{-methoxyphenyl})\text{-terpy}]Cl\}BPh_4$	HCT116 A2780	1.62 ± 0.05 9.69 ± 0.04	[6]
$\{Pt[4'-(4\text{-methoxynaphthalen-1-yl})\text{-terpy}]Cl\}CF_3SO_3$	HCT116 A2780	2.94 ± 0.03 16.12 ± 0.07	[6]
[Pt(4′-ferrocenyl-terpy)Cl]Cl	HaCaT (light) HaCaT (dark) MCF-7 (light) MCF-7 (dark)	12.0 ± 0.2 68.4 ± 0.3 12.2 ± 0.5 74.8 ± 1.1	[35]
[Pt{4′-[2-(piperidin-1-yl)etoxy]terpy}Cl]Cl	U2OS GM07575	61 ± 7 130 ± 12	[37]

[Pt{4′-[2-(morpholin-4-yl)etoxy]terpy}Cl]Cl	U2OS GM07575	95 ± 11 225 ± 26	[37]
$[Ru(dtpy)(dppz)Cl]^{+}$	HeLa dark HeLa light U2OS dark U2OS light 293T dark 293T light	79.4 ± 1.8 1.9 ± 0.4 79.4 ± 2.7 64.6 ± 3.1 40.7 ± 1.4 21.2 ± 1.2	[38]
$[Ru(dtpy)(dppz)CH_3CN]^{2+}$	HeLa dark HeLa light U2OS dark U2OS light 293T dark 293T light	34.4 ± 1.3 11.5 ± 0.7 57.5 ± 2.2 39.8 ± 2.1 37.5 ± 2.1 29.7 ± 0.8	[38]
$[Ru(pbpy)(addtpy)](ClO_4)$	HeLa normoxia HeLa hypoxia HeLa MCTSs A549 normoxia A549 hypoxia A549R normoxia A549R hypoxia L02 normoxia	1.05 ± 0.21 1.68 ± 0.25 3.26 ± 0.31 1.39 ± 0.21 1.86 ± 0.10 2.31 ± 0.16 2.54 ± 0.33 5.01 ± 0.41	[39]
$[Ru(terpy)(addtpy)](ClO_4)_2$	HeLa normoxia HeLa hypoxia HeLa MCTSs A549 normoxia A549 hypoxia A549R normoxia A549R hypoxia L02 normoxia	105.6 ± 5.37 122.6 ± 8.63 >200 112.5 ± 6.72 121.4 ± 4.57 113.6 ± 4.33 123.8 ± 8.62 129.5 ± 10.8	[39]
$[Ru(bbp)(addtpy)](ClO_4)_2$	HeLa normoxia HeLa hypoxia HeLa MCTSs A549 normoxia A549 hypoxia A549R normoxia A549R hypoxia L02 normoxia	22.46 ± 3.45 26.56 ± 1.65 60.45 ± 1.64 24.76 ± 2.31 30.70 ± 2.53 27.52 ± 2.04 29.64 ± 1.57 30.22 ± 1.63	[39]
$[Cu(dtpy)Cl_2]$	HeLa Bel-7402 HepG2	154 272 93	[40]

[Cu(pdtpy)Cl_2]	HeLa Bel-7402 HepG2	59 28 36	[41]
[Cu(adtpy)Cl_2]	HeLa Bel-7402 HepG2	39 21 27	[41]
[Cu(bfdtpy)Cl_2]	HeLa Bel-7402 HepG2	43 26 33	[41]
[Cu(fdtpy)Cl_2]	HCT116 A2780 A549	81.7 ± 0.3 5.9 ± 0.1 64.3 ± 0.3	[42]
[Cu(tdtpy)Cl_2]	HCT116 A2780 A549 MCF7	20.5 ± 0.4 4.6 ± 0.1 22.6 ± 0.3 62.3 ± 0.5	[42]
[Cu(mpdtpy)Cl_2]	A2780 A549 MCF7	2.6 ± 0.1 70.1 ± 0.4 89 ± 0.5	[42]

dtpy = 2,6-di(thiazo1-2-yl)pyridine; **dppz** = dipyrido[3,2-a:2′,3′-c]phenazine; **addtpy** = 2-(2,6-di(thiazol-2-yl)pyridin-4-yl)anthracene-9,10-dione; **pbpy** = 6-phenyl-2,2’-bipyridine; **terpy** = 2,2′:6′,2″-terpyridine; **bbp** = 2,6-bis(benzimidazol-2-yl)pyridine; **pdtpy** = 4-phenyl-2,6-di(thiazole-2-yl)pyridine; **adtpy** = 4-(anthracen-9-yl)-2,6-di(thiazole-2-yl)pyridine; **bfdtpy** = 4-(benzofuran-2-yl)-2,6-di(thiazole-2-yl)-pyridine; **fdtpy** = 4-(furan-2-yl)-2,6-di(thiazole-2-yl)pyridine; **tdtpy** = 4-(thiophen-2-yl)-2,6-di(thiazole-2-yl)pyridine; **mpdtpy** = 4-(1-methyl-1H-pyrrol-2-yl)-2,6-di(thiazole-2-yl)pyridine.

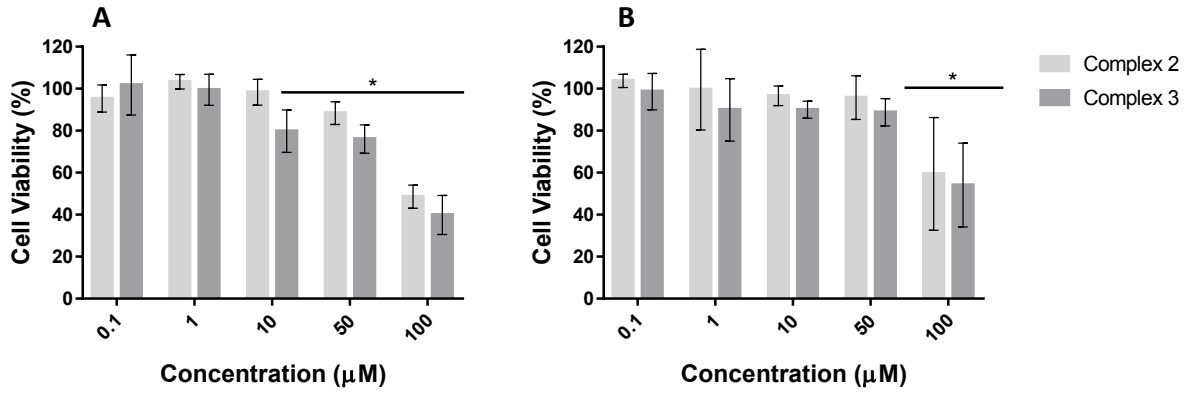

Figure S12. Cytotoxicity of complexes **2** and **3** in PC3 (A) and MCF7 (B) cancer cell lines and evaluated after 48 h of exposure to increasing concentrations of each complex. Cell viability percentage was determined by the MTS method. DMSO 0.1% (v/v) was used as vehicle control condition. The results presented are average ± SD of three independent assays. The symbol * indicates that p-value <0.05

Table S13. Values of relative IC_{50} (µM) of complexes (**2**) and (**3**) in A2780 cancer line after 24 h exposure to the complexes. The results presented are average ± SD of three independent assays

Cell line	**2** (µM)	**3** (µM)
A2780	14.5± 0.2	7.1 ± 0.1

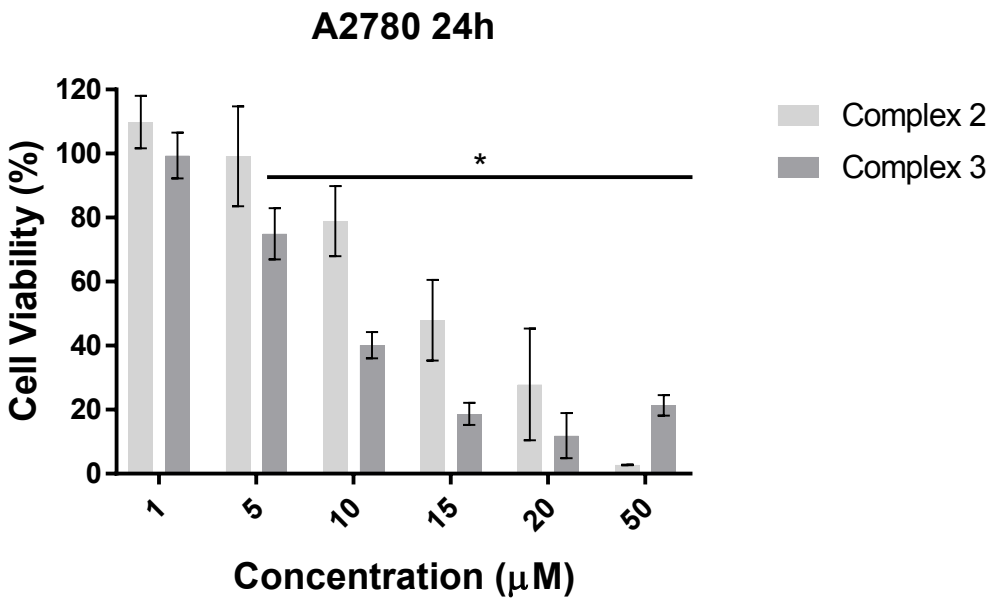

Figure S13. Cytotoxicity of ligands complexes (**2**) and (**3**) in A2780 cancer cell line evaluated after 24 h exposure to increasing concentrations of each. Cell viability percentage was determined by the MTS method. DMSO 0.1% (v/v) was used as vehicle control condition. The results presented are average ± SD of three independent assays. The symbol * indicates that p-value <0.05

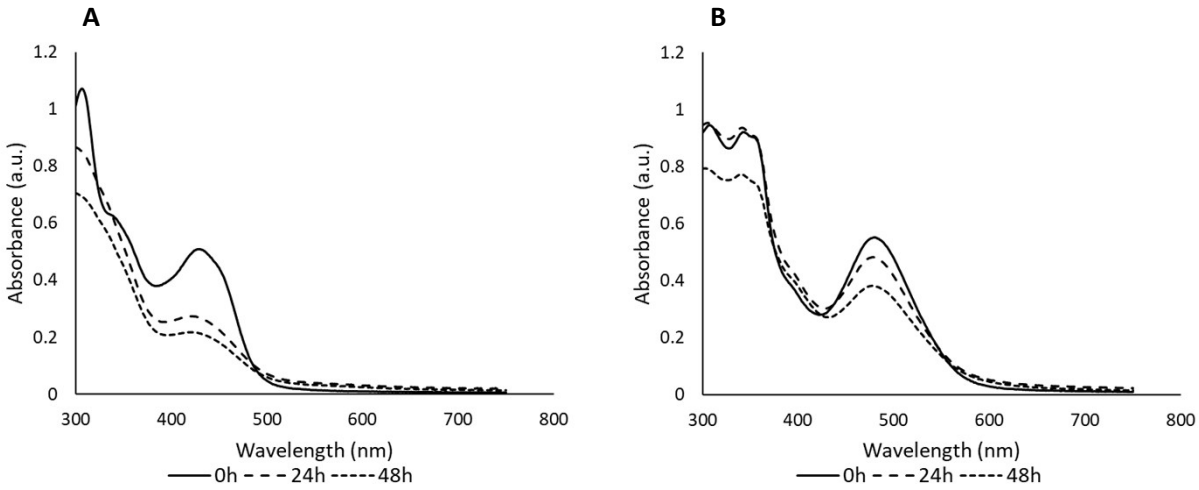

Figure S14. Variation of absorption spectra (300-800 nm) of 50 µM of Pt(II) (**2**) (A) and (**3**) (B) evaluated after incubation at 37 °C for 24 h and for 48 h in DMEM medium. The absorption spectra of 50 µM of Pt(II) complexes **2** (A) and **3** (B) in DMEM at time 0 was used as reference.

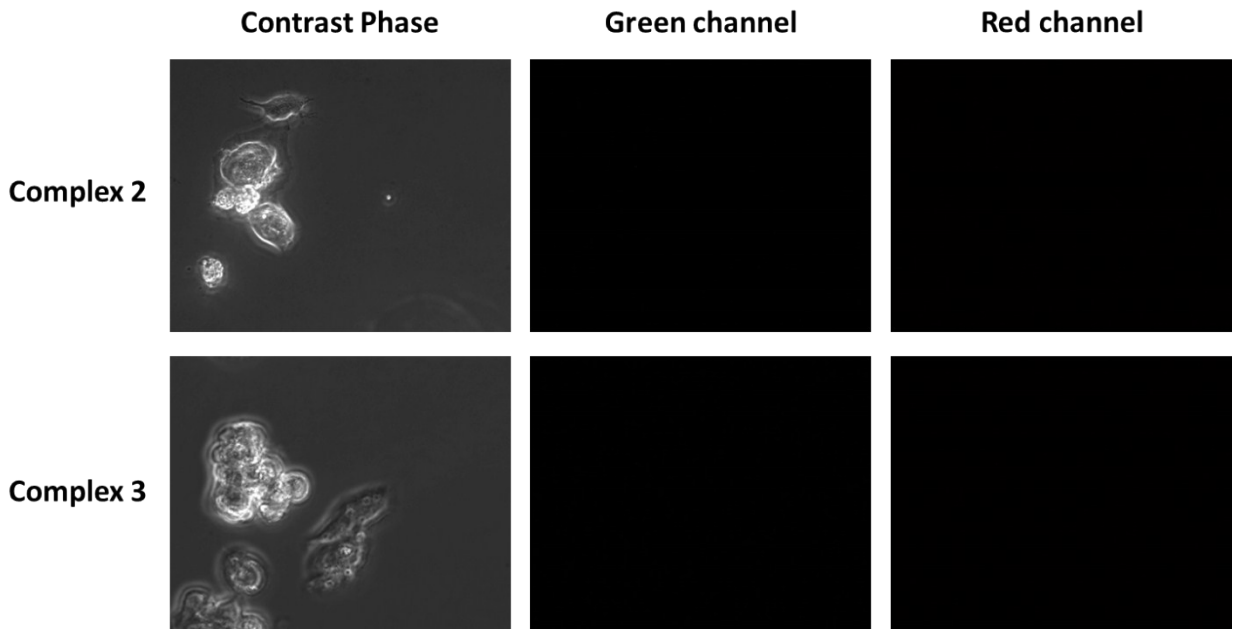

Figure S15. Representative images of controls without JC-1 stain of A2780 cells exposed to IC_{50} concentrations of complexes (**2**) and (**3**), subjected to the same conditions as the assays used for mitochondrial membrane potential analysis.

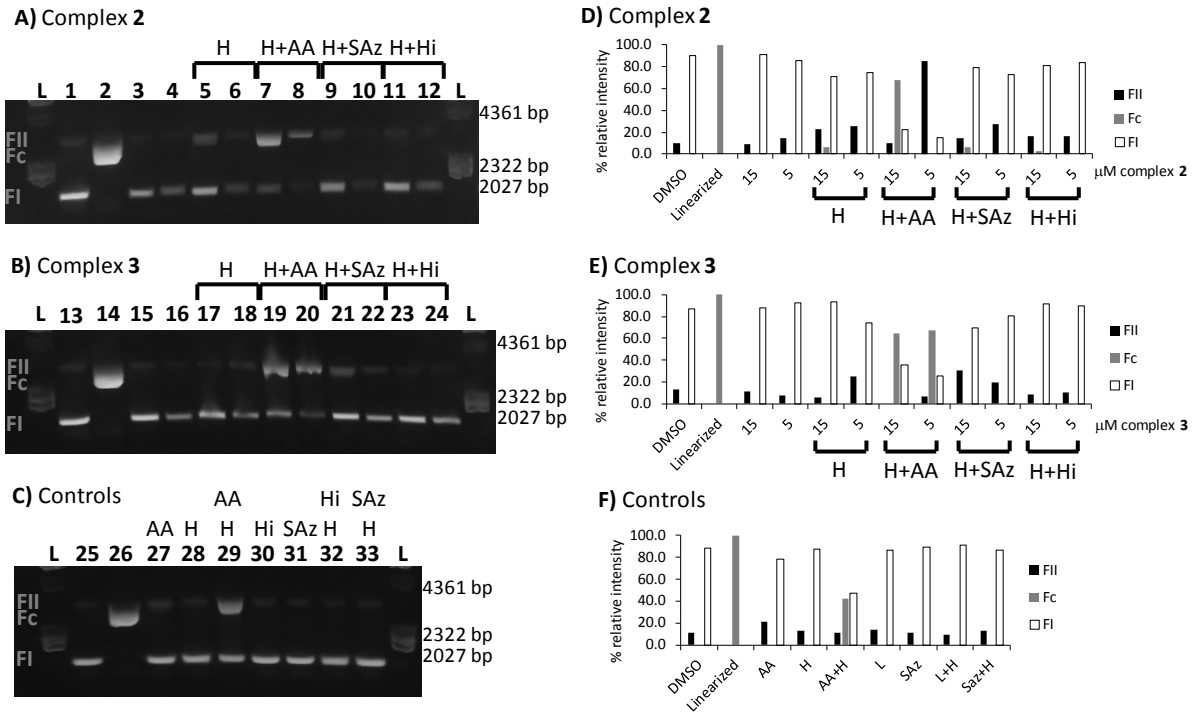

Figure S16. Agarose gel electrophoresis (0.8 % (w/v)) to study the interaction of complexes (**2**) (A) and (**3**) (B) with 100 ng pUC18 plasmidic DNA (pDNA) in the presence and absence of 100 mM H_2O_2 (H) and the reductants ascorbic acid (AA, 50 mM), Sodium azide (SAz, 50 mM) or L-Histidine (Hi, 50 mM). For this analysis, an incubation period of 24h at 37ºC was used. (C) Effect of 100 mM H_2O_2 and reductants in pUC18. Lane L – Molecular ladder LDNA/HindIII; lanes 1, 13 and 25 – pUC18 incubated with 0.01 %(v/v) DMSO; lanes 2, 14 and 26 – linearized pUC18; lane 3 - pUC18 incubated with 15 µM complex **2**; lane 4 - pUC18 incubated with 5 µM complex **2**; lane 5 - pUC18 incubated with 15 µM complex **2** and 100 mM H_2O_2; lane 6 - pUC18 incubated with 5 µM complex **2** and 100 mM H_2O_2; lane 7 - pUC18 incubated with 15 µM complex **2**, 100 mM H_2O_2 and 50 mM ascorbic acid; lane 8 - pUC18 incubated with 5 µM complex **2**, 100 mM H_2O_2 and 50 mM ascorbic acid; lane 9 - pUC18 incubated with 15 µM complex **2**, 100 mM H_2O_2 and 50 mM sodium azide; lane 10 - pUC18 incubated with 5 µM complex **2**, 100 mM H_2O_2 and 50 mM sodium azide; lane 11 - pUC18 incubated with 15 µM complex **2**, 100 mM H_2O_2 and 50 mM L-Histidine; lane 12 - pUC18 incubated with 5 µM complex **2**, 100 mM H_2O_2 and 50 mM L-Histidine; lane 15 - pUC18 incubated with 15 µM complex **3**; lane 16 - pUC18 incubated with 5 µM complex **3**; lane 17 - pUC18 incubated with 15 µM complex **3** and 100 mM H_2O_2; lane 18 - pUC18 incubated with 5 µM complex **3** and 100 mM H_2O_2; lane 19 - pUC18 incubated with 15 µM complex **3**, 100 mM H_2O_2 and 50 mM ascorbic acid; lane 20 - pUC18 incubated with 5 µM complex **3**, 100 mM H_2O_2 and 50 mM ascorbic acid; lane 21 - pUC18 incubated with 15 µM

complex **3**, 100 mM H_2O_2 and 50 mM sodium azide; lane 22 - pUC18 incubated with 5 μM complex **3**, 100 mM H_2O_2 and 50 mM sodium azide; lane 23- pUC18 incubated with 15 μM complex **3**, 100 mM H_2O_2 and 50 mM L-Histidine; lane 24 - pUC18 incubated with 5 μM complex **3**, 100 mM H_2O_2 and 50 mM L-Histidine; lane 27 - pUC18 incubated with 50 mM ascorbic acid; lane 28 - pUC18 incubated with 100 mM H_2O_2; lane 29 - pUC18 incubated with 50 mM ascorbic acid and 100 mM H_2O_2; lane 30 - pUC18 incubated with 50 mM L-Histidine; lane 31 - pUC18 incubated with 50 mM sodium azide; lane 32 - pUC18 incubated with 100 mM H_2O_2 and 50 mM L-Histidine; lane 33 - pUC18 incubated with 100 mM H_2O_2 and 50 mM sodium azide. D) Percentage of band intensity of each pDNA isoform in A); E) Percentage of band intensity of each pDNA isoform in B); Percentage of band intensity of each pDNA isoform in C) Fl – supercoiled isoform of pDNA (White bars); Fc – linear (double strand breaks) isoform of pDNA (grey bars); FII – relaxed (nicked) isoform of pDNA (black bars).

REFERENCES

[1] Yip, H.-K.; Cheng, L.-K.; Cheung, K.-K.; Che, C.-M. *J. Chem. Soc., Dalton Trans.*, **1993**, 2933

[2] Buchner, R.; Cunningham, C. T.; Field, J. S.; Haines, R. J.; McMillin, D. R.; Summerton, G. C., *J. Chem. Soc., Dalton Trans.*, **1999**, 711

[3] Maroń, A.; Szłapa, A.; Czerwińska, K.; Małecki, J. G.; Krompiec, S.; Machura, B. *CrystEngComm*, **2016**, *18*, 5528

[4] Huo, J.; Arulsamy, N.; Hoberg, J. O. *Dalton Trans.*, **2011**, *40*, 7534

[5] Field, J. S.; Wilson, C. R.; Munro, O. Q. *Inorg. Chim. Acta*, **2011**, *374*, 197

[6] Maron, A.; Czerwińska, K. A.; Machura, B.; Raposo, L. R.; Rodrigues, C.; Fernandes, A.; Malecki, J.; Szłapa-Kula, A.; Kula, S.; Krompiec, S. *Dalton Trans.*, **2018**, *47*, 6444

[7] Malecki, J. G. CSD Communication (Private Communication), **2014**

[8] Zou, H.-H.; Wang, L.; Long, Z.-X.; Qin, Q.-P.; Song, Z.-K.; Xie, T.; Zhang, S.-H.; Liu, B. Lin, Y.-C.; Chen, Z.-F. *Eur. J. Med. Chem.*, **2016**, *108*, 1

[9] Sakuda, E.; Funahashi, A.; Kitamura, N. *Inorg.Chem.*, **2006**, *45*, 10670

[10] Yutaka, T.; Mori, I.; Kurihara, M.; Mizutani, J.; Tamai, N.; Kawai, T.; Irie, M.; Nishihara, H. *Inorg. Chem.*, **2002**, *41*, 7143

[11] Wadas, T. J.; Wang, Q.-M.; Kim, Y.-j.; Flaschenreim, C.; Blanton, T. N.; Eisenberg, R. *J. Am. Chem. Soc.*, **2004**, *126*, 16841

[12] Du, P.; Han, A.; Sun, Z.; Wu, H.; Yan, Z.; Jia, H.; Zhang, R.; Liang, Z.; Cao, R.; Eisenberg, R. *Inorg. Chem.*, **2014**, *53*, 3338

[13] Zhang, G.; Li, Q.; Fu, W.; Wang, D. *Acta Crystallogr., Sect. E: Struct. Rep. Online*, **2010**, *66*, m681

[14] Field, J. S.; Gertenbach, J.-A.; Haines, R. J.; Ledwaba, L. P.; Mashapa, N. T.; McMillin, D. R.; Munro, O. Q.; Summerton, G. C. *Dalton Trans.*, **2003**, *0*, 1176

[15] Field, J. S.; Haines, R. J.; McMillin, D. R.; Summerton, G. C. *J. Chem. Soc., Dalton Trans.*, **2002**, *0*, 1369

[16] Maroń, A.; Czerwińska, K.; Małecki, J. G.; Machura, B.; Szłapa-Kula, A.; Krompiec, S. *Chem. Sel.*, **2017**, *2*, 1071

[17] Malecki, J. G. CSD Communication (Private Communication), **2017**

[18] Lazzaro, D. P.; Fanwick, P. E.; McMillin, D. R. *Inorg. Chem.*, **2012**, *51*, 10474

[19] Guo, F.; Sun, W. *J. Phys. Chem. B*, **2006**, *110,* 15029-15036

[20] Michalec, J. F.; Bejune, S. A.; Cuttell, D. G.; Summerton, G. C.; Gertenbach, J. A.; Field, J. S.; Haines, R. J.; McMillin, D. R. *Inorg. Chem.*, **2001**, *40,* 2193

[21] Michalec, J. F.; Bejune, S. A.; McMillin, D. R. *Inorg. Chem.*, **2000**, *39,* 2708

[22] Anbalagan, V.; Srivastava, T. S. *J. Photochem. Photobiol. A*, **1995**, *89*, 113

[23] Naik, A.; Rubbiani, R.; Gasser, G., Spingle, B. *Angew. Chem.*, **2014**, *126*, 7058

[24] McKenzie, L. K.; Bryant, H. E.; Weinstein, J. A. *Coord. Chem. Rev.*, **2019**, *379*, 2

[25] Doherty, R. E.; Sazanovich, I. V.; McKenzie, L. K.; Stasheuski, A. S.; Coyle, R.; Baggaley, E.; Bottomley, S.; Weinstein, J. A.; Bryant, H. E. *Sci. Rep.*, *6*, 22668/ doi: 10.1038/srep22668

[26] Xue, X.; Zhu, C.; Chen, H.; Bai, Y.; Shi, X.; Jiao, Y.; Chen, Z.; Miao, Y.; He, W.; Guo, Z. *Inorg. Chem.*, **2017**, *56*, 3754

[27] Potocny, A. M.; Pistner, A. J.; Yap, G. P. A.; Rosenthal, J. *Inorg. Chem.*, **2017**, *56*, 12703

[28] Ramu, V.; Gautam, S.; Garai, A.; Kondaiah, P.; Chakravarty, A. R. *Inorg. Chem.*, **2018**, *57*, 1717

[29] Djurovich, P. I.; Murphy, D.; Thompson, M. E.; Hernandez, B.; Gao, R.; Hunt, P. L.; Selke, M. *Dalton Trans.*, **2007**, *0*, 3763

[30] Anbalagan, V.; Srivastava, T. S.; *J. Photochem. Photobiol. A*, **1994**, *77*, 141

[31] Shavaleev, N. M.; Adams, H.; Best, J.; Edge, R.; Navaratnam, S.; Weinstein, J. A. *Inorg. Chem.*, **2006**, *45*, 9410

[32] Lai, S.-W.; Liu, Y.; Zhang, D.; Wang, B.; Lok, C.-N.; Che, C.-M.; Selke, M. *Photochem. Photobiol.*, **2010**, *86*, 1414

[33] Lowe, G.; Droz, A. S.; Vilaivan, T.; Weaver, G. W.; Park, J. J.; Pratt, J. M.; Tweedale, L.; Kelland, L. R. *J. Med. Chem.*, **1999**, *42*, 3167

[34] Bligh, S. W. A.; Bashall, A.; Garrud, C.; McPartlin, M.; Wardle, N.; White, K.; Padhye, S.; Barve, V.; Kundu, G. *Dalton Trans.,* **2003**, *0*, 184

[35] Mitra, K.; Basu, U.; Khan, I.; Maity, B.; Kondaiah, P.; Chakravarty, A. R. *Dalton Trans.*, **2014**, *43*, 751

[36] Wang, S.; Chu, W.; Wang, Y.; Liu, S.; Zhang, J.; Li, S.; Wei, H.; Zhou, G.; Qin, X. *Appl. Organometal. Chem.*, **2013**, *27*, 373

[37] Stafford, V. S.; Suntharalingam, K.; Shivalingam, A.; White, A. J. P.; Mann, D. J.; Vilar, R. *Dalton Trans.*, **2015**, *44*, 3686

[38] Yu, H.-j.; Liu, J.-p.; Hao, Z.-f.; He, J.; Sun, M.; Hu, S.; Yu, L.; Chao, H. *Dyes Pigm.*, **2017**, *136*, 416

[39] Zeng, L.; Chen, Y.; Huang, H.; Wang, J.; Zhao, D.; Ji, L.; Chao, H. *Chem. Eur. J.*, **2015**, *21*, 15308

[40] Li, G.-Y.; Du, K.-J.; Wang, J.-Q.; Liang, J.-W.; Kou, J. –F.; Hou, X.-J.; Ji, L.-N.; Chao, H. *J. Inorg. Biochem.*, **2013**, *119*, 43

[41] Li, L.; Du, K.; Wang, Y.; Jia, H.; Hou, X.; Chao, H.; Ji, L. *Dalton Trans.*, **2013**, *42*, 11576

[42] Czerwińska, K.; Machura, B.; Kula, S.; Krompiec, S.; Erfurt, K.; Roma-Rodrigues, C.; Fernandes, A. R.; Shul'pina, L. S.; Ikonnikov, N. S.; Shul'pin, G. B. *Dalton Trans*., **2017**, *46*, 9591